AD-A033 280 METEOROLOGY RESEARCH INC ALTADENA CALIF F/G 4/2
PMS PRECIPITATION PROBE INTER-COMPARISONS AND CORRELATIONS WITH--ETC(U)
FEB 76 E LOBL, A J HEYMSFIELD, R E CARBONE DNA001-75-C-0040
UNCLASSIFIED MRI-76-FR-1400 DNA-3992F NL

| OF |
AD
A033280

END

DATE
FILMED
2-77

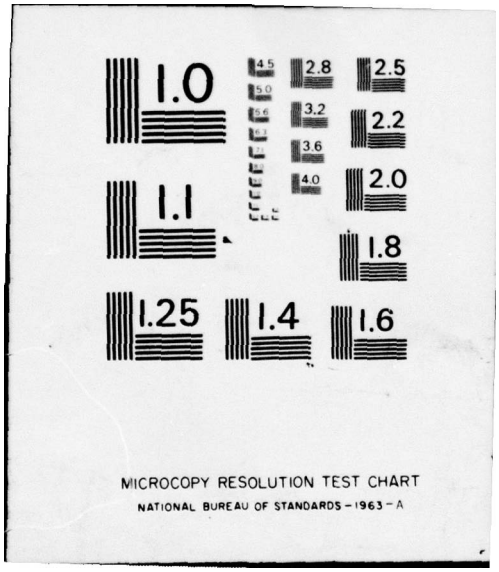
1.0
1.1
1.25
1.4
1.6
1.8
2.0
2.2
2.5
2.8
3.2
3.6
4.0
4.5
5.0
MICROCOPY RESOLUTION TEST CHART
NATIONAL BUREAU OF STANDARDS - 1963 - A

(12)

NWDNA 3992F

PMS PRECIPITATION PROBE INTERCOMPARISONS AND CORRELATIONS WITH RADAR MEASUREMENTS

Meteorology Research, Inc.
464 West Woodbury Road
Altadena, California 91001

27 February 1976

Final Report

CONTRACT No. DNA 001-75-C-0040

THIS WORK SPONSORED BY THE DEFENSE NUCLEAR AGENCY
UNDER RDT&E RMSS CODE B342075462 L37HAXYX91022 H2590D.

Prepared for

Director
DEFENSE NUCLEAR AGENCY
Washington, D. C. 20305

Destroy this report when it is no longer needed. Do not return to sender.

UNCLASSIFIED

SECURITY CLASSIFICATION OF THIS PAGE *(When Data Entered)*

REPORT DOCUMENTATION PAGE	READ INSTRUCTIONS BEFORE COMPLETING FORM
1. REPORT NUMBER: DNA 3992F	2. GOVT ACCESSION NO. / 3. RECIPIENT'S CATALOG NUMBER
4. TITLE *(and Subtitle)*: PMS PRECIPITATION PROBE INTER-COMPARISONS AND CORRELATIONS WITH RADAR MEASUREMENTS.	5. TYPE OF REPORT & PERIOD COVERED: Final Report, 1
	6. PERFORMING ORG. REPORT NUMBER: MRI-76-FR-1400
7. AUTHOR(s): E. Lobl, R. E. Carbone, A. J. Heymsfield, L. J. Jahnsen	8. CONTRACT OR GRANT NUMBER(s): DNA 001-75-C-0040
9. PERFORMING ORGANIZATION NAME AND ADDRESS: Meteorology Research, Inc. 464 West Woodbury Road Altadena, California 91001	10. PROGRAM ELEMENT, PROJECT, TASK AREA & WORK UNIT NUMBERS: Subtask L37HAXYX910-22
11. CONTROLLING OFFICE NAME AND ADDRESS: Director Defense Nuclear Agency Washington, D.C. 20305	12. REPORT DATE: 27 Feb[illegible] 1976
	13. NUMBER OF PAGES: 62
14. MONITORING AGENCY NAME & ADDRESS *(if different from Controlling Office)*	15. SECURITY CLASS *(of this report)*: UNCLASSIFIED
	15a. DECLASSIFICATION/DOWNGRADING SCHEDULE

16. DISTRIBUTION STATEMENT *(of this Report)*

Approved for public release; distribution unlimited.

17. DISTRIBUTION STATEMENT *(of the abstract entered in Block 20, if different from Report)*

18. SUPPLEMENTARY NOTES

This work sponsored by the Defense Nuclear Agency under RDT&E RMSS Code B342075462 L37HAXYX91022 H2590D.

19. KEY WORDS *(Continue on reverse side if necessary and identify by block number)*

Hydrometeor-Size Spectra
Particle Measuring System Probe Comparisons

20. ABSTRACT *(Continue on reverse side if necessary and identify by block number)*

Two versions of PMS precipitation probes are compared from simultaneous spectrum measurements. Systematic probe differences reveal undersizing and depth-of-field problems with the "wide-arm" (4500 μm) probe. Radar comparisons with the aircraft data substantiate the deduced problems and quantitative correction procedures are developed and demonstrated for the "wide-arm" probe. Instances of very large radar discrepancies are shown to be caused in part by poor selection of particle phase and/or habit.

DD FORM 1 JAN 73 1473 EDITION OF 1 NOV 65 IS OBSOLETE

UNCLASSIFIED

SECURITY CLASSIFICATION OF THIS PAGE *(When Data Entered)*

227 500

TABLE OF CONTENTS

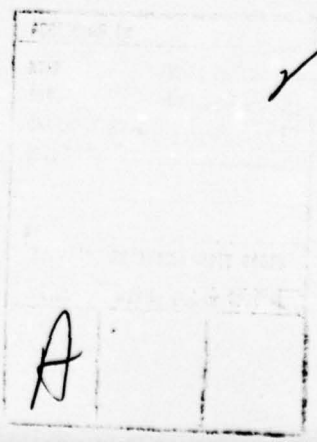

1. INTRODUCTION

The accuracy of ice crystal size spectra measurements using the Particle Measuring Systems (PMS) spectrometers has been a source of considerable uncertainty in recent years. The two existing versions differ primarily in their resolution (R). Special flights made by the Meteorology Research, Inc. (MRI) Citation and Navajo indicated a systematic difference between the two probe types (Davey, 1975). Ground tests were conducted with the probes mounted on the WB-57F and the Citation by Thompson Ramo Woolridge (TRW). In addition, tests were performed by PMS to determine the sizing effect of the probes. These tests were performed on rectangular and circular optical arrays for both the narrow- and wide-arm precipitation spectrometers.

Cunningham (1975) reported that the "wide-arm" precipitation probe (WAP) measurements result in calculated equivalent radar reflectivity factor underestimates from 5 to 15 dBZ[1]. Calculations by other investigators using the "narrow-arm" version of the PMS precipitation probe (NAP) measurements found agreement to better than 5 dBZ with the radar data.

Davey (1975) concluded, from a comparison with foil and replicator data, that NAP was more accurate in ice than in liquid water precipitation.

The true limitations and uncertainties of the PMS precipitation probes in ice clouds are beginning to be uncovered. Heymsfield (1975) and Carbone and Srivastava (1975) have studied ice clouds with simultaneous aircraft and Doppler radar observations. They calculated radar reflectivity factor (obtained from a NAP installed on a WB-57F) and found that it agreed quite closely with the radar measurements. Above

[1] dBZ = 10 log Z, where Z is the radar reflectivity factor

5 km the true reflectivity factors were within 2 dBZ with the discrepancy increasing to 6.1 dBZ at 2.6 km. The conclusion from the above discussion is that NAP measurements are generally in better agreement with radar than the WAP measurements. The excellent agreement found by Heymsfield and Srivastava suggests that, when comparing the two probes, NAP can be used as a "control" probe provided the maximum particle size does not greatly exceed probe sizing capability.

There are three factors which contribute to the discrepancy between aircraft and radar measurements.

1. Maximum particle size (typically between 1 and 2 mm) which the NAP is capable of measuring. The existing particles larger than L_{max} at the lower levels of an ice cloud can account for part of the discrepancy.

2. Crystal light transmission problem. Crystals with thin edges and finely divided branches generally do not shadow sufficiently and result in undersizing. Nondimensional corrections (Knollenberg, 1975) for different crystal habits were developed and are currently available but do not explain observed discrepancies.

3. Mass-length relationships. The mass-length relationships found by Heymsfield (1972) and Locatelli and Hobbs (1974) were used in the calculations. Any inaccuracies in these assumptions introduce errors in the calculated reflectivity factors. This problem is currently under investigation by Cunningham, Knollenberg, and Heymsfield with preliminary results indicating this to be a secondary effect.

In the present work, data from NAP and WAP were compared. Calculated reflectivity factors from these data were then compared to

the (ALCOR) radar measurements taken simultaneously with the aircraft data.

2. TEST PROCEDURES AND DATA PROCESSING

2.1 Test Procedures

Correlation flights, simultaneous aircraft and radar measurements, were made over Kwajalein in September and October 1974. The two versions of the PMS Optical Array Precipitation Probes (WAP - wide-arm probe, NAP - narrow-arm probe) were mounted on a C-130E aircraft. WAP was equipped with spherical photodiodes, while NAP had rectangular ones. On October 12, 1974 excellent data was available for constant level passes between 4.8 and 8.8 km, at 1 km intervals.

The radar was in a tracking link-offset mode, sampling a cloud volume approximately 3 km ahead of the C-130E. The radar used in this study is the ALCOR C-band, which transmits a frequency modulated "chirp" pulse. Its characteristics are:

λ	= 5.29 cm
h_e (effective pulse depth)	= 37.5 m
θ (beam width)	= 0.005 rad

2.2 Data Processing

2.2.1 Data Processing at AFGL

Particle spectra, water content (WC) and radar reflectivity factor (Z) were calculated by scientists at Air Force Geophysical Laboratories (AFGL) from aircraft tapes. Particle spectra data for both probes were processed in a similar manner: the results are presented as 4-second averages. The Knollenberg (Kn) corrections, necessary to adjust for the crystal light transmission problem, were applied. The ice crystal habits

chosen for processing were based on either replicator observations, snow stick or assumptions of growth habits which occur at a given temperature. The ALCOR data were available in 1-second averages.

2.2.2 *Data Processing at MRI*

WC and Z values were reprocessed at MRI using the basic particle spectra obtained by AFGL with different crystal habits, i.e., crystal habits that seemed more realistic given spatial continuity considerations from state parameters and radar measurements. The Kn corrections applied to sample spectra are listed in Table 1.

The maximum crystal size measurable with the NAP was 1.85 mm and with the WAP, 4.5 mm. Only the data below 1.85 mm were taken into consideration, even when other data existed.

2.3 Other Considerations

Three important considerations in comparing radar-measured with aircraft-calculated reflectivity factor should be discussed at this point.

1. The sampling volume of the radar, as used in the present configuration, was 10^5 to 10^6 m^3, while the PMS probes sampling volume was only 0.1 m^3 per second. The factor of 10^6 to 10^7 difference results in a smoothing out of gradients in reflectivity factor as measured by the radar when compared to aircraft data. Averaging the data over an interval of time will result in a smoothing to some degree of the aircraft data also.

TABLE 1. KNOLLENBERG CORRECTION FACTORS TO PMS PROBES FOR DIFFERING HYDROMETEOR TYPES

I (Actual Size Class) = X + YI (Measured Size Class)

Hydrometeor Type	X	Y
	Spherical Photodiodes	
Rain	0.22	0.99
Plates	0.16	1.07
Branched Dendrites	0.72	1.03
Columns	1.50	1.10
Bullet Rosettes	0.40	1.01
Large and Small Snow	0.18	1.15
	Rectangular Photodiodes	
Rain	0.36	1.03
Plates	0.51	1.08
Branched Dendrites	1.24	1.03
Columns	1.39	1.26
Bullet Rosettes	0.69	1.04
Large and Small Snow	0.75	1.16

2. It is very difficult to convert radar return power and aircraft size spectra measurements into radar reflectivity factors in regions within or just below the melting level since an uncertaintly exists in the hydrometeor types in the region.

3. The NAP sampling volume is a factor of 6 lower than the WAP. The small sampling volumes of the probes, resulting in a truncation of concentrations lower than about 100 m^{-3} for WAP will affect radar reflectivity calculations where large particles in small concentrations exist.

3. PARTICLE SPECTRA AND DEDUCED PMS PROBE LIMITATIONS

Comparison of data measured with NAP and WAP indicates large discrepancies in particle concentrations. In rain, these discrepancies occur mostly at the small size end of the spectrum. In snow and ice crystals the entire WAP measured spectrum is shifted with respect to the NAP data. From previous research, and radar data in the present study it was concluded that NAP data usually resulted in reflectivity factors close to radar measurements and, therefore, the NAP could be used as a "control" probe. Correction factors that bring the WAP spectra into closer agreement with the NAP spectra are sought. The method of approach to the problem is an iterative one. Basically, the method consists of qualitatively examining various spectra from both probes to determine the sense, magnitude and circumstances surrounding the largest discrepancies. Following careful examination of many spectra (measured by probes simultaneously) two major problems are suspected: (1) undersizing due to high crystal light transmission (UNSZ) by the thin parts of the ice crystal and (2) undercounting due to depth of field limitations --

a small volume in which particles in the first few size classes are not in focus (hereinafter referred to as DF). It is useful to discuss the effects of these problems with respect to hypothetical model spectra before application of corrections to actual measured spectra.

3.1 Model Spectra

Both UNSZ and DF problems are discussed in this section. Model spectra are used to illustrate and quantify the individual problems. Observations show two principal forms of particle size spectra: (1) exponential, decreasing with increasing ice crystal size, and (2) bimodal, decreasing exponentially from the second peak with increasing size. Besides these two spectral forms, the spectra may be characterized as either "narrow" (to ~ 0.5 mm) or "wide" (to 2-3 mm). It is instructive to see the changes in the spectral form which result from the aforestated problems.

3.1.1 Exponential Spectrum

Figure 1 illustrates how a narrow, exponential spectrum changes due to UNSZ and/or DF problems. Figure 1a shows an original spectrum and a spectrum shifted 1.5 size classes to the left: a case of UNSZ. The loss in the total particle concentration due to this undersizing is more than 90 percent, the first, the most populated, size class has disappeared completely and only half of the second one is still present. Figure 1b illustrates the effect of a pure DF problem. The two cases presented are: $DF \propto R$ and $DF \propto R^2$, with channel 4 in complete focus. Note that in this case the spectrum appears undercounted. This problem is not nearly as severe as the UNSZ illustrated in 1a; however, 70 percent of the total number concentration is lost in the "$DF \propto R^2$" case. Figure 1c shows the effect of combining DF and UNSZ on a narrow exponential spectrum. Note here, the extreme case of "$DF \propto R^2$" where only 0.5 percent of the total number concentration remains.

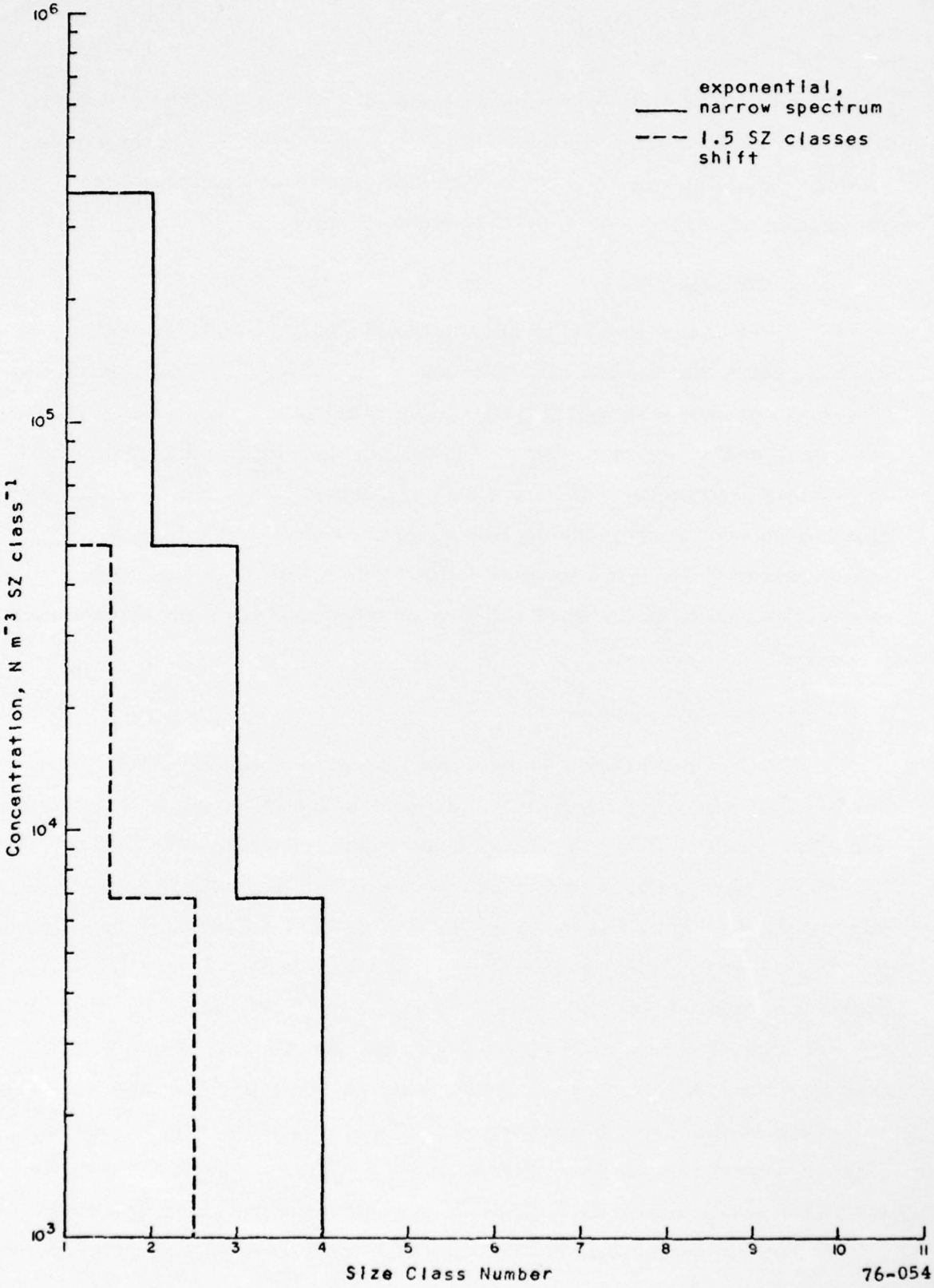

Figure 1a. Narrow exponential model spectrum with UNSZ problem

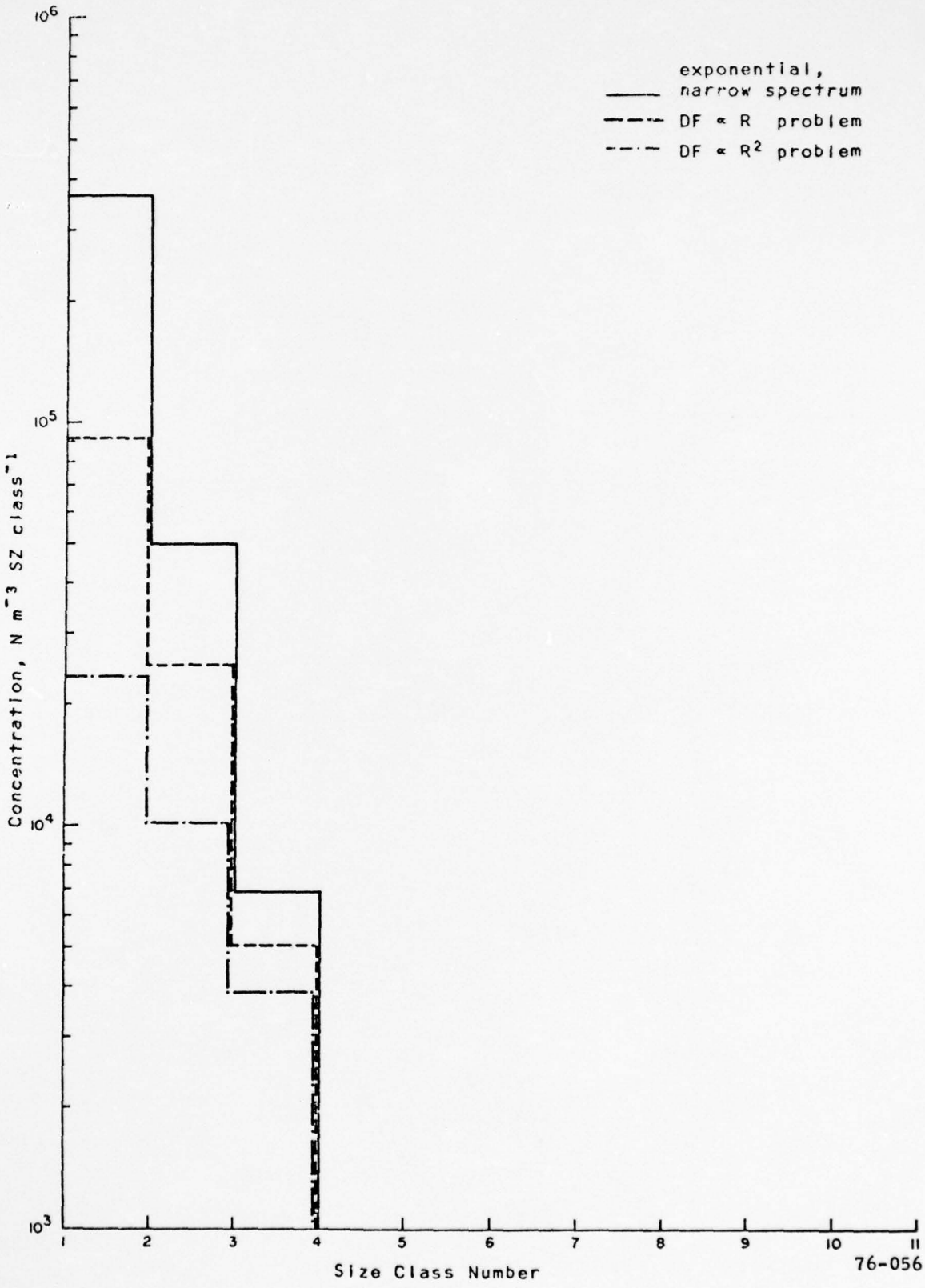

Figure 1b. Narrow exponential model spectrum with DF problem

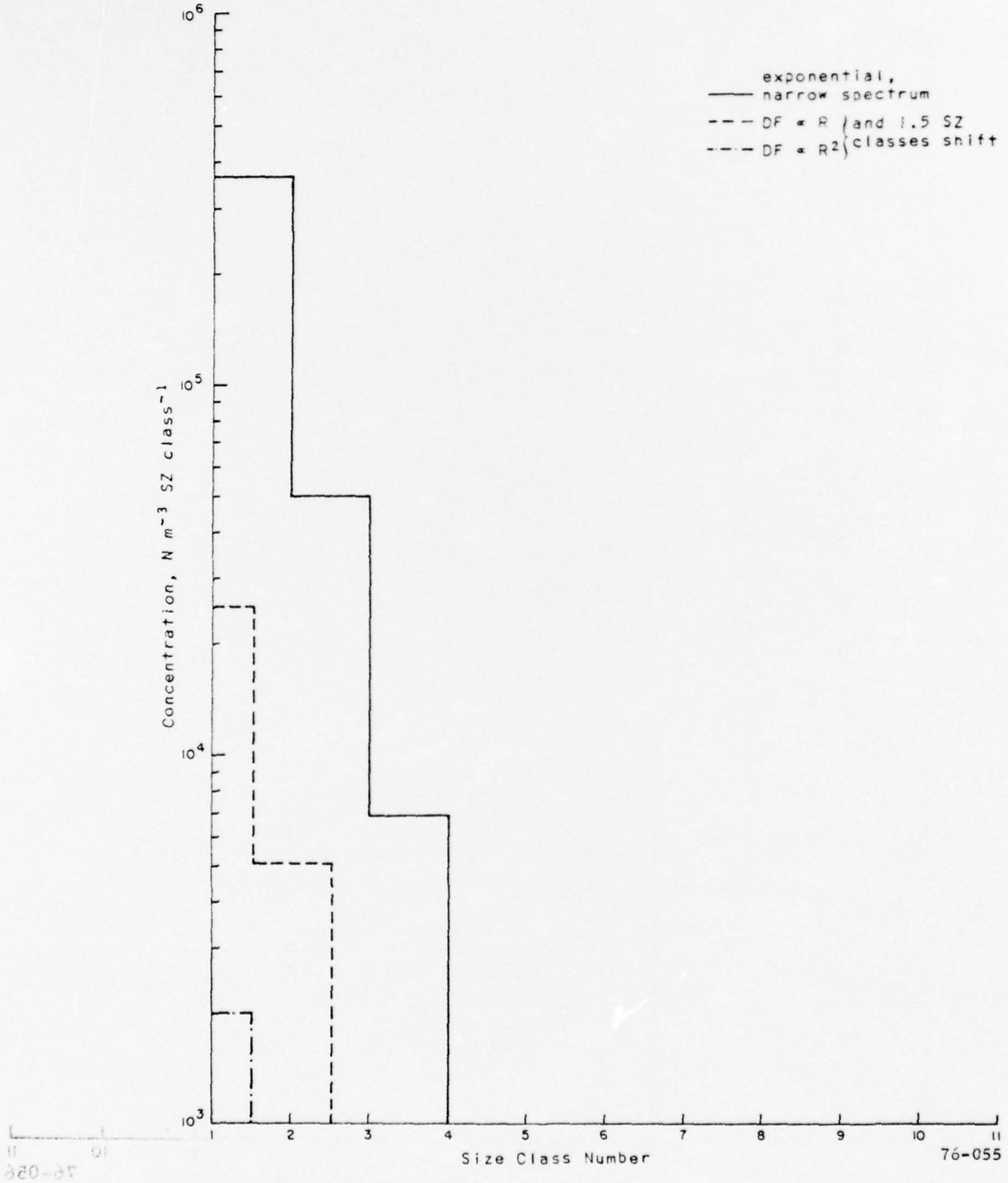

Figure 1c. Narrow exponential model spectrum with UNSZ and DF problems

Figure 2 illustrates the changes that can occur with a wide, exponential spectrum if UNSZ and/or DF problems are present. Figure 2a shows the case of a shift in the actual spectrum of 1.5 size classes to the left. Note that even though there is some undersizing, this problem generally would not produce an underestimate in Z and WC of the magnitude commonly observed. The 50 percent reduction in total number concentration in the sample spectrum shown produces a 5 dBZ difference in the reflectivity factor. When DF is the only problem as in Figure 2b, there is no undersizing but an undercounting at the smaller sizes which causes the spectrum to change from its truly exponential character. Figure 2c shows the combined effect of both DF and UNSZ problems.

3.1.2 Bimodal Spectrum

In general, the UNSZ problem alone affects the total number and size of the particles. The DF problem changes the spectral form such that a bimodal spectrum becomes an exponential or monomodal.

Figure 3 shows the effects of these problems on a narrow bimodal spectrum. Figure 3a shows that a pure shift keeps the bimodal spectrum intact. The shape of the spectrum will change, however, if the shift is sufficiently large to eliminate the first peak. If DF is the only problem, as in Figure 3b, the tail end of the spectrum does not change, however, the small end becomes severely underestimated (by 55 percent in the "$DF \propto R$" case and by 65 percent in the "$DF \propto R^2$ case). Figure 3c illustrates the effect of both DF and UNSZ.

Figures 4a, b, and c show the effects of UNSZ and DF on a wide bimodal spectrum. The results are similar to the effects on the narrow spectrum, with a higher percentage of particles lost in this case.

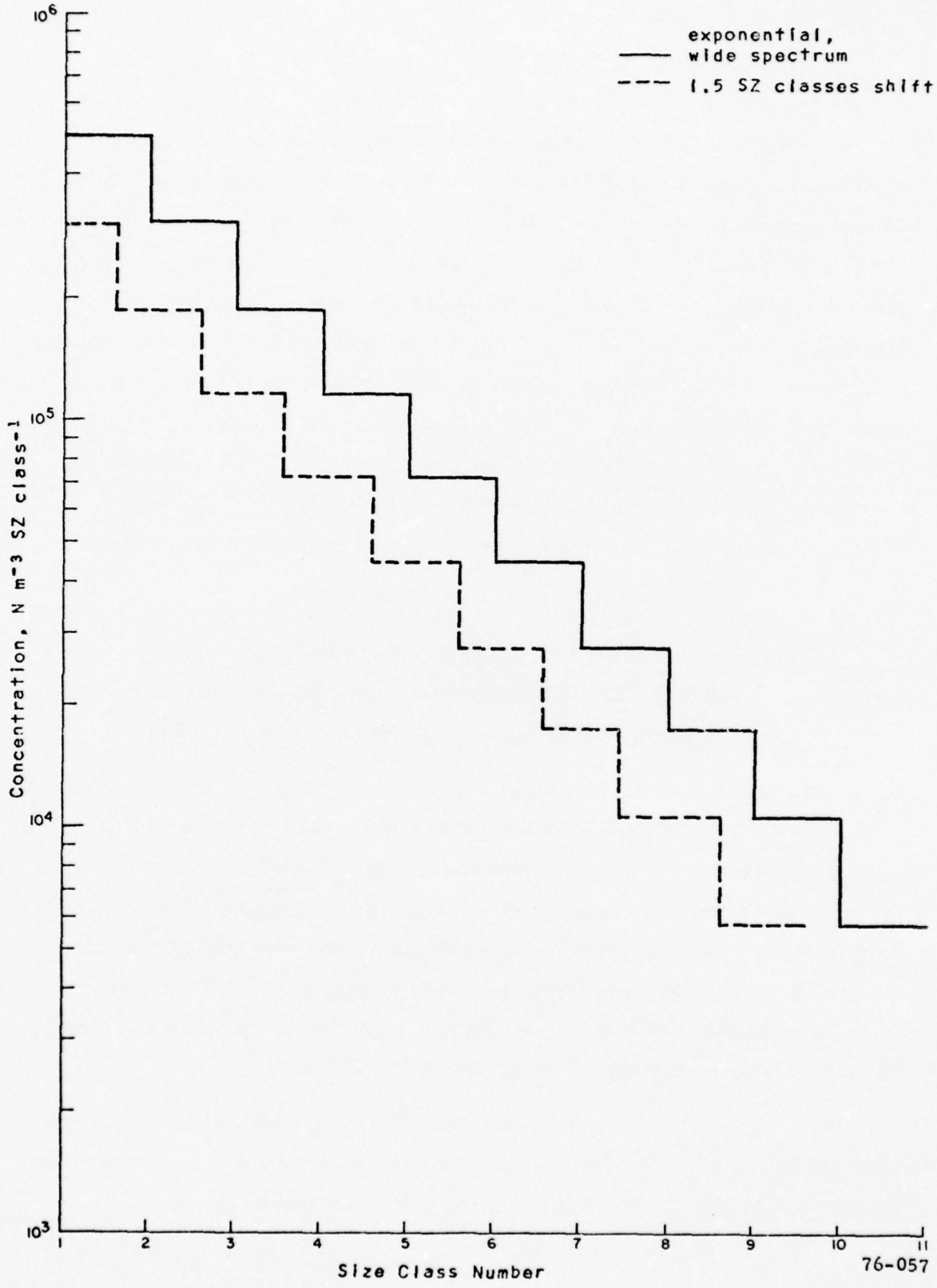

Figure 2a. Wide exponential model spectrum with UNSZ problem

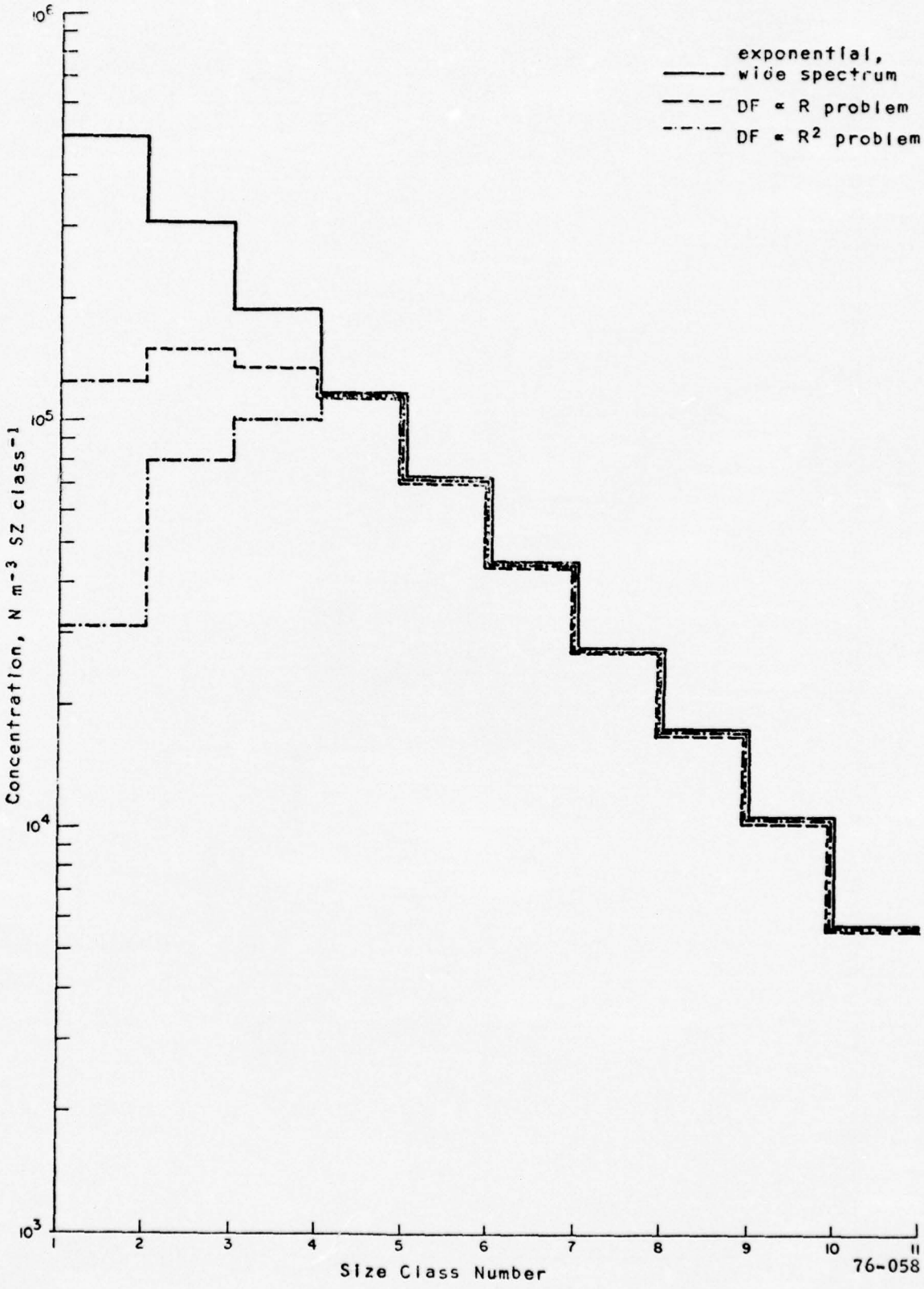

Figure 2b. Wide exponential model spectrum with DF problem

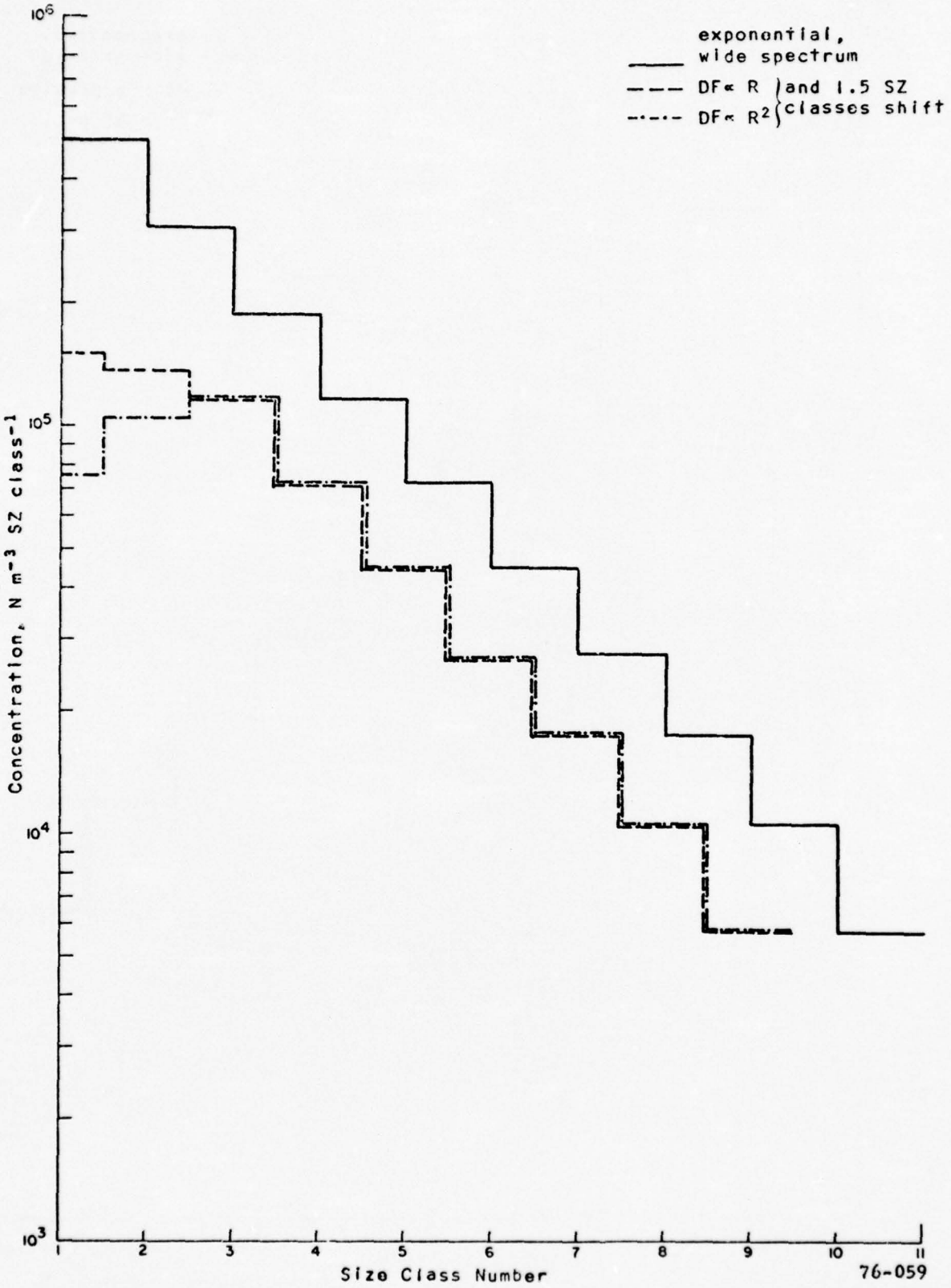

Figure 2c. Wide exponential model spectrum with UNSZ and DF problems

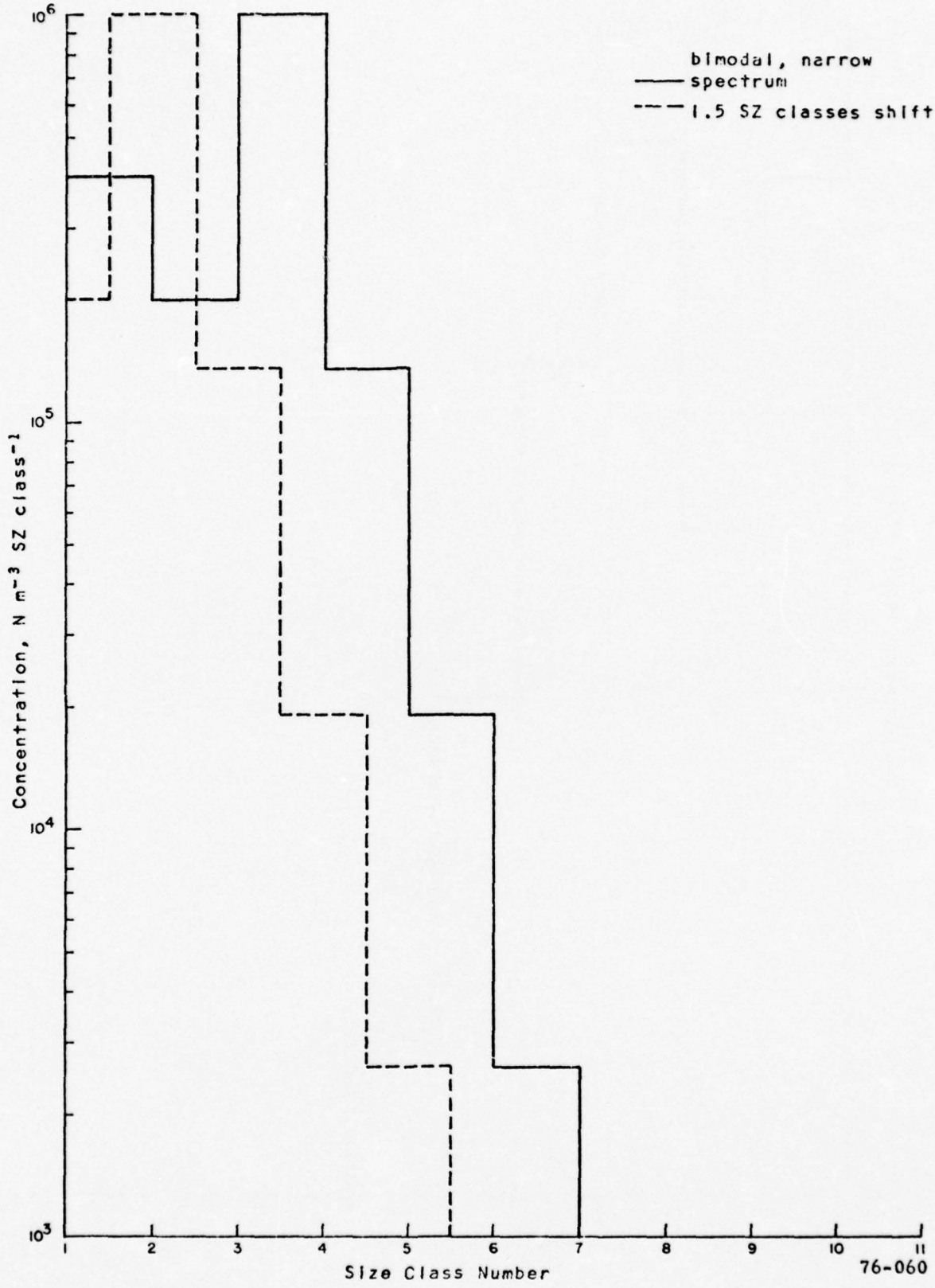

Figure 3a. Narrow bimodel model spectrum with UNSZ problem

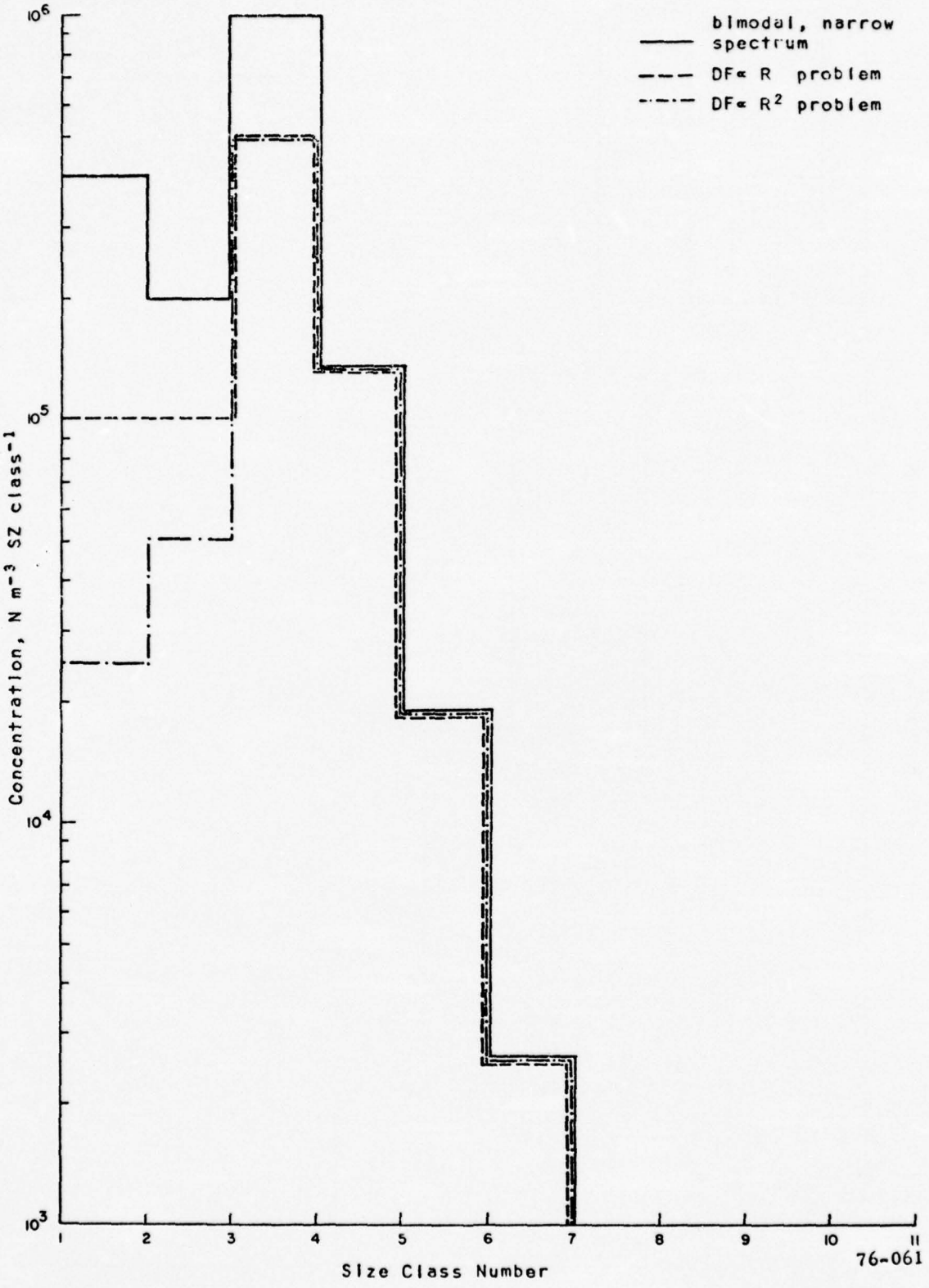

Figure 3b. Narrow bimodal model spectrum with DF problem

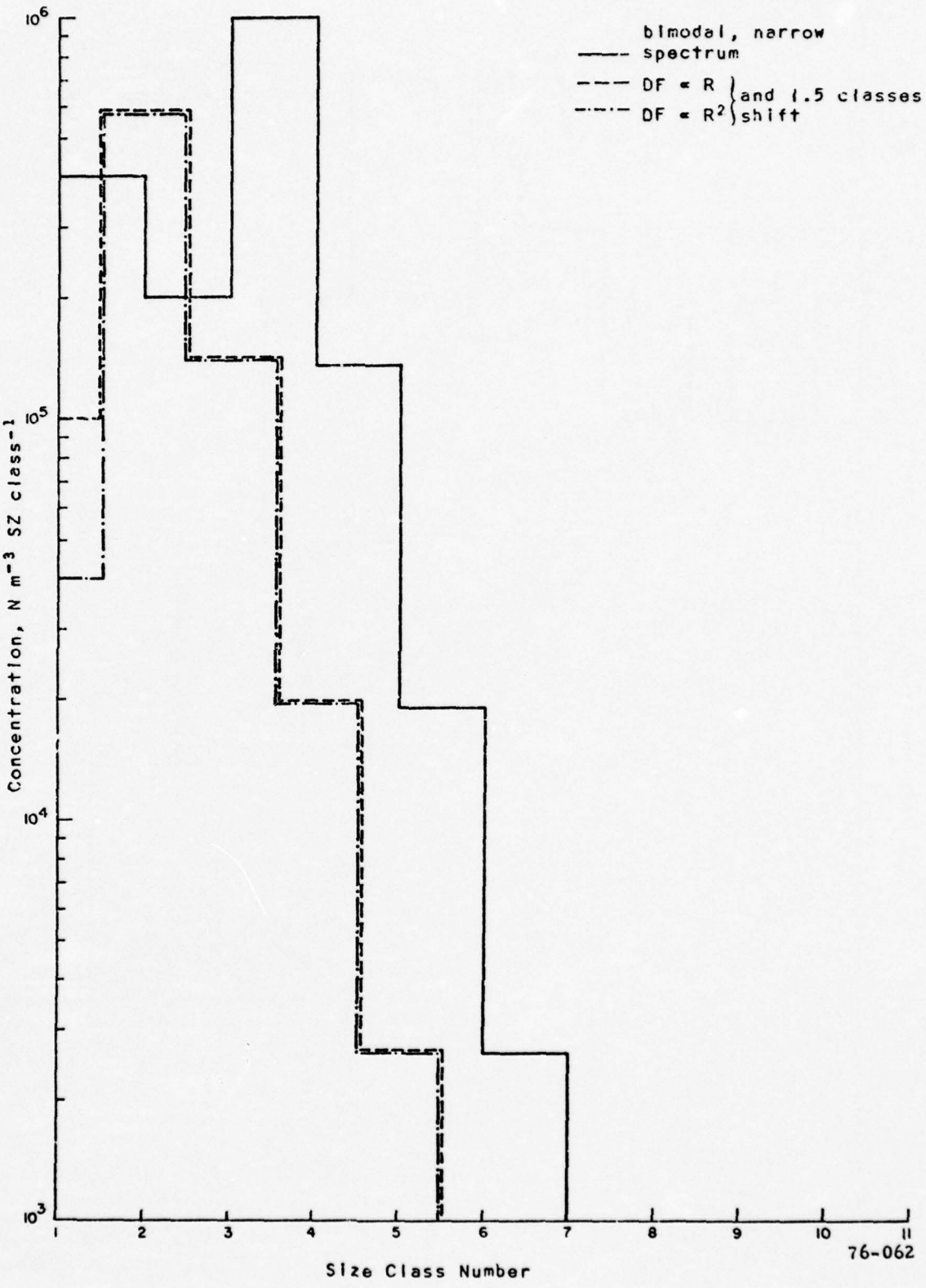

Figure 3c. Narrow bimodal model spectrum with UNSZ and DF problems

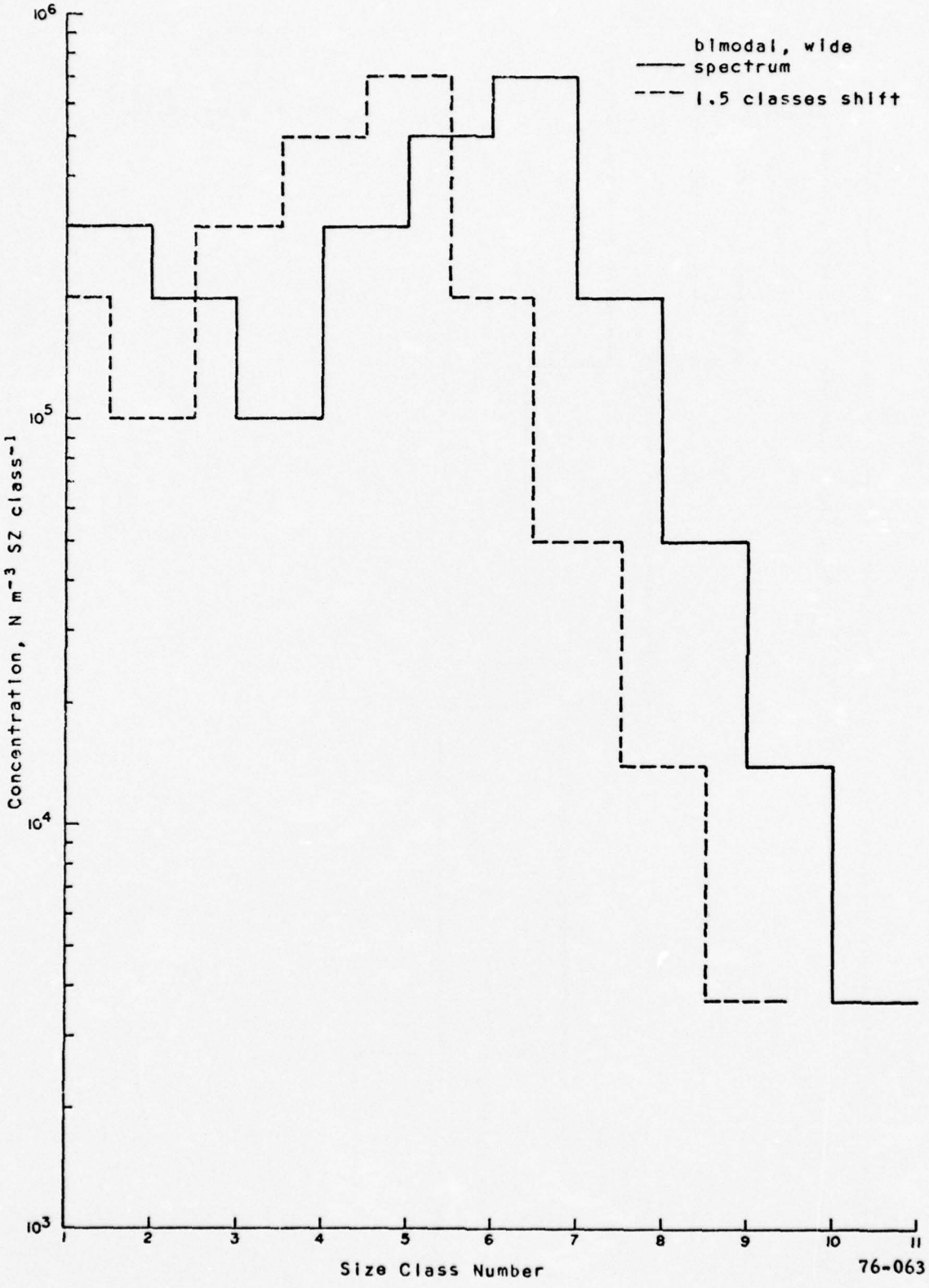

Figure 4a. Wide bimodal model spectrum with UNSZ problem

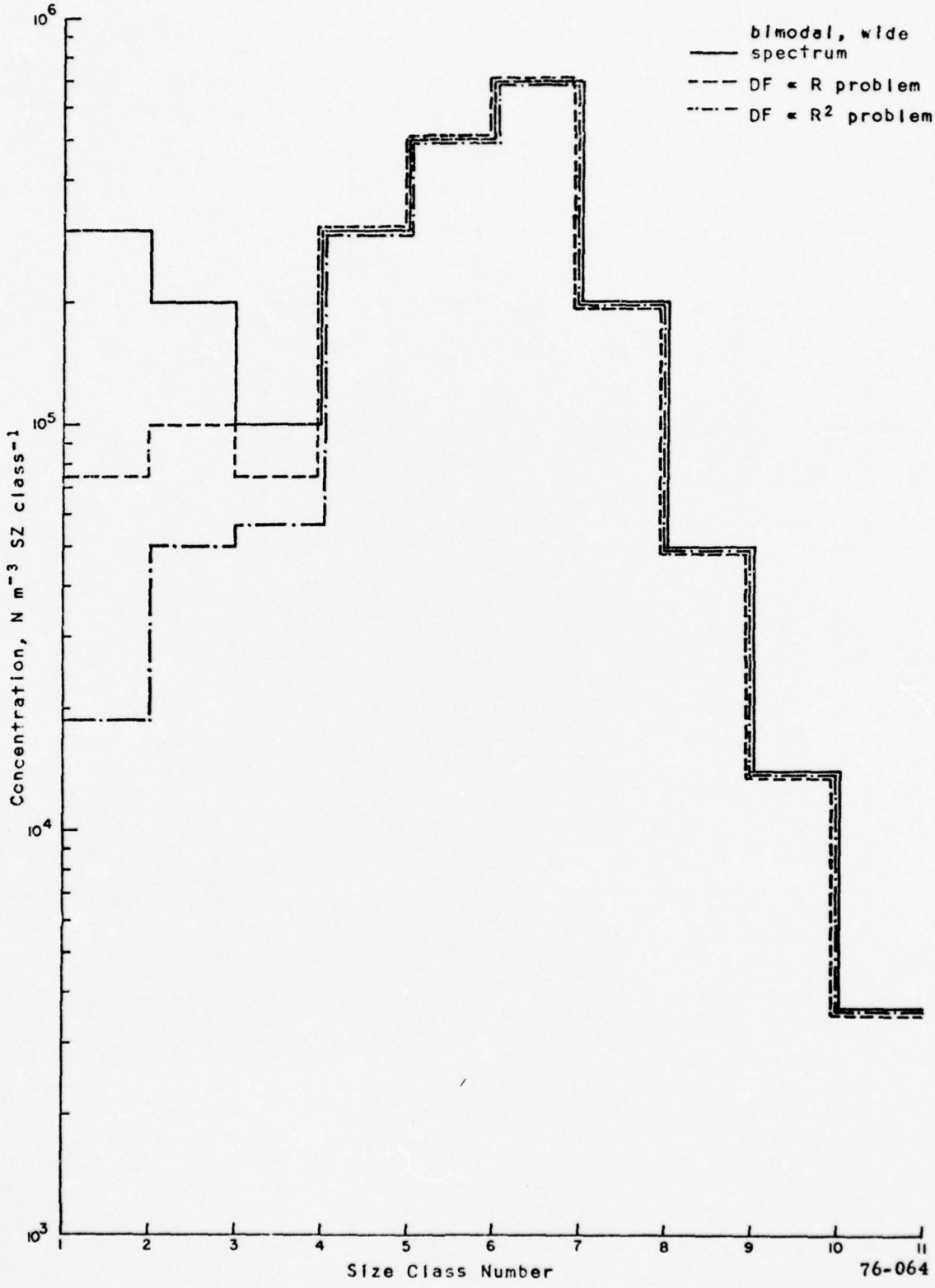

Figure 4b. Wide bimodal model spectrum with DF problem

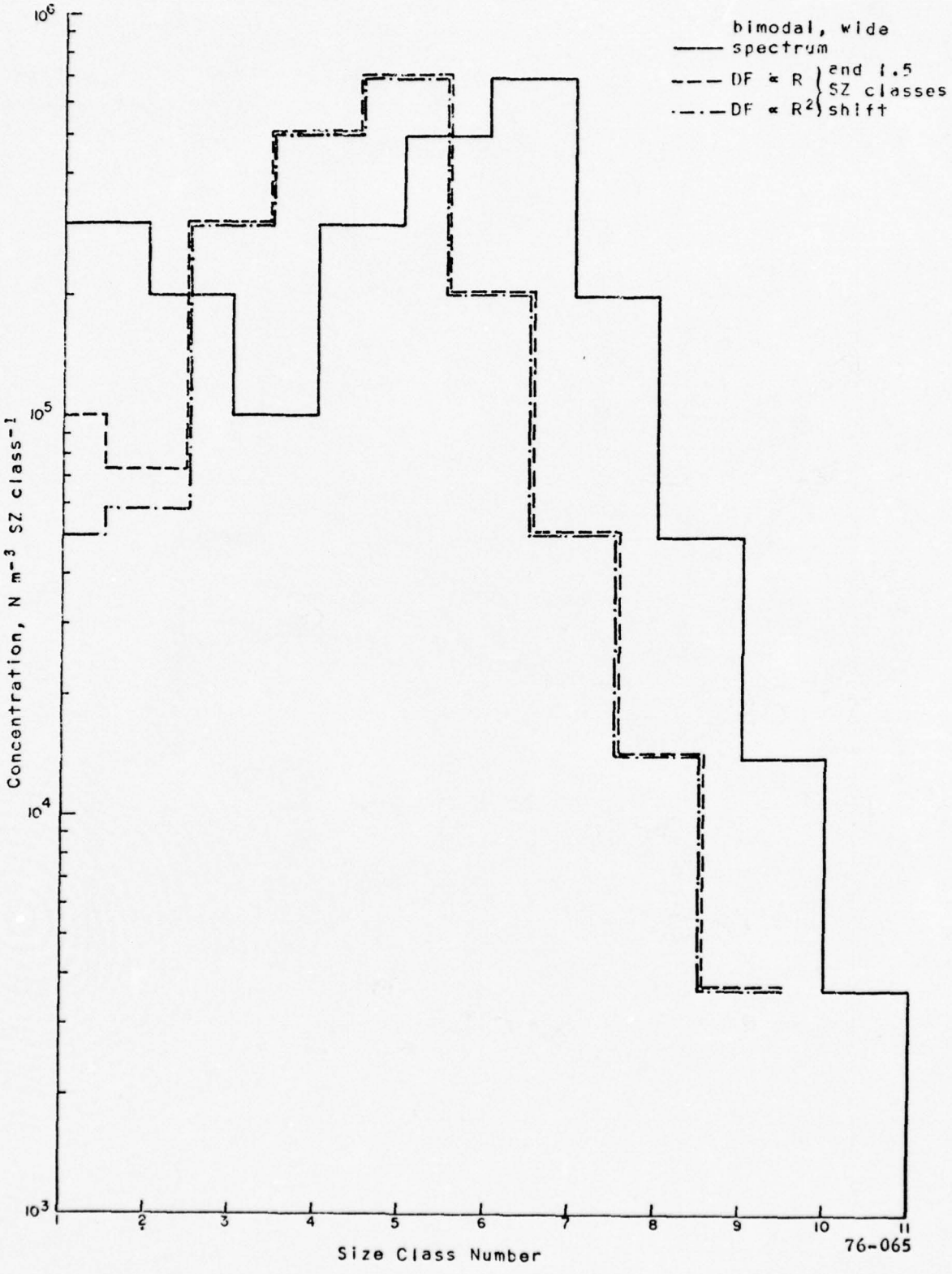

Figure 4c. Wide bimodal model spectrum with UNSZ and DF problems

3.2 Deduced Correction Factors: Depth of Field and Undersizing

3.2.1 Undersizing Correction

Undersizing commonly occurs with ice particles that have thin branches or edges. These parts do not shadow sufficiently and thus they are not "seen" by the probe. This problem appears to occur at all sizes with about the same magnitude, hence the slope of a spectrum of undersized particles is parallel to the real spectral slope. In the case of WAP and NAP, NAP is considered the "control" probe. The distance between the slopes of the measured spectra (by the two probes) is the shift. The correction applied to the aforementioned spectra were only approximations to the nearest half-size-class. It will be seen in Section 4.2 that the shift is habit dependent: no shift for rain and maximum shift for small snow and bullet rosette spectra.

Quantitatively, for pure exponential spectra one can write:

$$N_1 = N_{01}\, e^{-\Lambda_1 L}$$

$$N_2 = N_{02}\, e^{-\Lambda_2 L}$$

where N is the number concentration, Λ, the spectrum slope, and L, the length of the particles measured.

When $\Lambda_1 = \Lambda_2 \equiv \Lambda$ and $N_1 = N_2$, then

$$N_{01}\, e^{-\Lambda L_1} = N_{02}\, e^{-\Lambda L_2}$$

or
$$L_1 - L_2 \equiv \Delta L = \frac{1}{\Lambda}\, \ell n\, \frac{N_{01}}{N_{02}} \qquad (1)$$

Expression (3) is a formula for obtaining the exact amount of undersizing or shift. In general, the undersizing of the WAP data was from 0 to 2 size classes, or up to 0.6 mm.

3.2.2 Depth of Field Correction

The WAP measurements also suffer from an undercounting problem, especially at the small sizes. The corrections applied were such as to make the WAP spectrum slope parallel to the NAP one. They were either proportional to the resolution, R, of the probe, in the case of ice particles, or proportional to R^2, in the case of rain.

This undercounting problem is largely due to the depth of field limitations. The WAP has 26.3 cm separation between its arms where small particles cannot possibly be in focus over this entire distance. The small particles close to one arm will not be counted because they will not be in focus. One can find the distance midway between the arms where different size particles are in focus.

$$\text{DIF (cm)} = K\ L\ \text{(cm)} \qquad (2)$$

where DIF is the "distance in focus", K is a probe characteristic constant and L is the length of the particle in question. The maximum DIF is 26.3 cm. Assume that the third size class particles are always in focus. The minimum length of the particles in focus is 3 × 0.03 cm Thus

$$26.3 = K \times 3 \times 0.03 = 3\,K\,R$$

$$K = \frac{26.3}{3\,R}$$

Then the DIF for any size particle is:

$$\text{DIF} = 292\ L$$

For example, a crystal 0.01 cm long will be in focus only in the 2 cm interval, midway between the probe arms. The undercounting in this case, assuming a constant concentration of particles, is more than 90 percent.

The following sections apply UNSZ and DF corrections as previously described to actual measured spectra.

4. PRECIPITATION PROBE COMPARISON

4.1 Particle Spectra

Figures 5 and 6 are examples of rain spectra. The original data have similarly shaped spectra: exponential spectra for NAP data, and an almost flat, or a small slope, for WAP spectra. The DF corrections applied changed the WAP spectra such that they coincided with the NAP spectra. In these cases, there were no UNSZ corrections needed. In both cases, an R^2 (R is the probe resolution) DF correction was applied. The size of the particles first in focus (SZF) differed from day to day (perhaps due to different instrumentation setup procedures).

Figures 7 and 8 represent two spectra for wet snow. Both NAP spectra are bimodal. The WAP spectra (when compared to the NAP spectra) suffer from both UNSZ and DF problems. The UNSZ problem is severe in Figure 7. The shift due to the undersizing is approximately one size class (300 μm). The undercounting of particles in the first size class is obvious (the spectra flattens); the WAP does not "see" all the small particles that exist in the sampling volume. This DF problem is corrected by assuming an R dependence of the depth of field. The NAP and the corrected WAP spectra now have similar slopes, and the horizontal distance between them is the shift (UNSZ shift).

Figure 9 illustrates a "large snow" spectrum. Both UNSZ and DF problems are again present: the undersizing is approximately one-half size class, the DF correction is proportional to R, and SZF is approximately 900 μm.

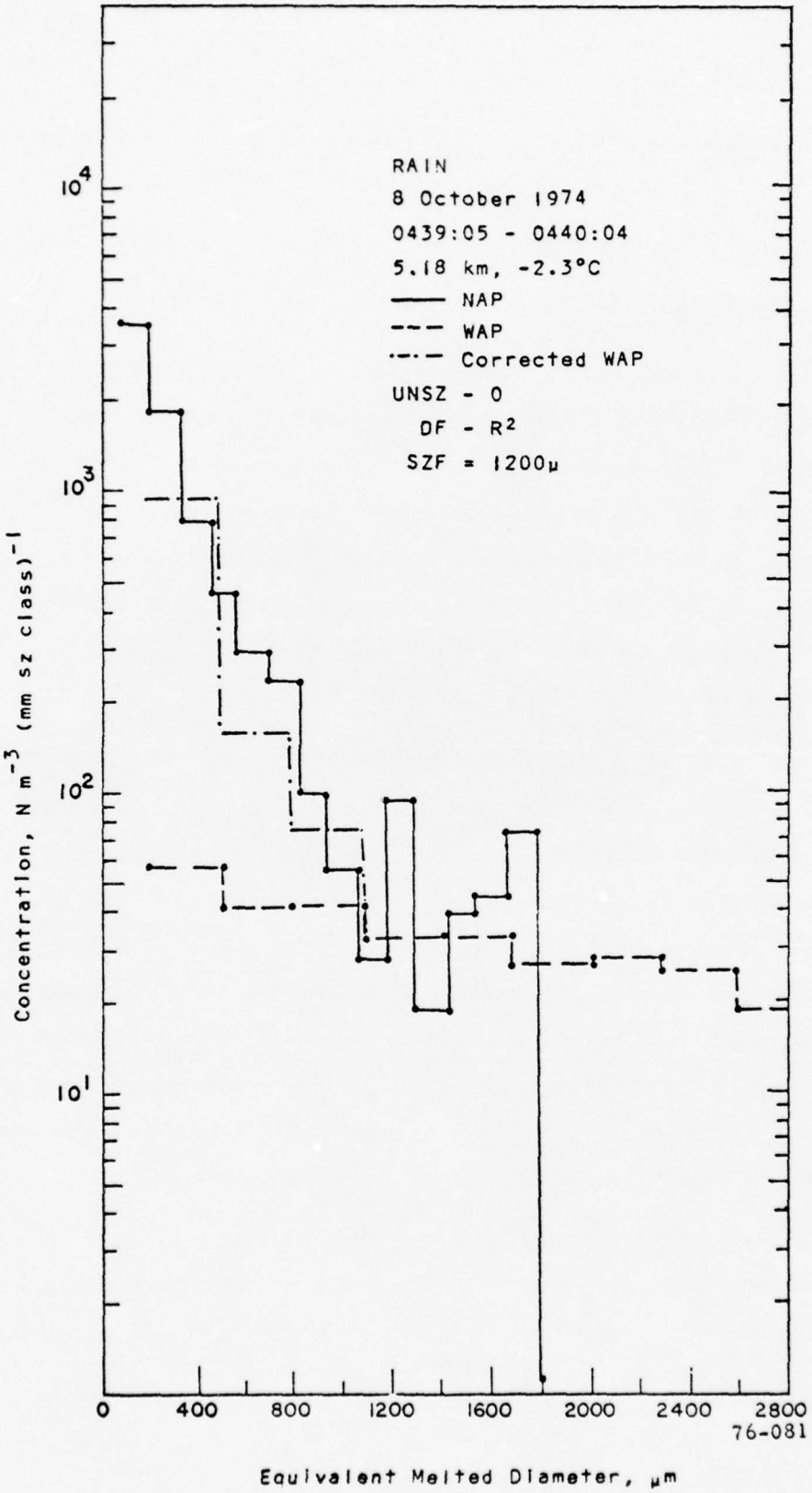

Figure 5. Comparative rain spectra and corrections as indicated in legend

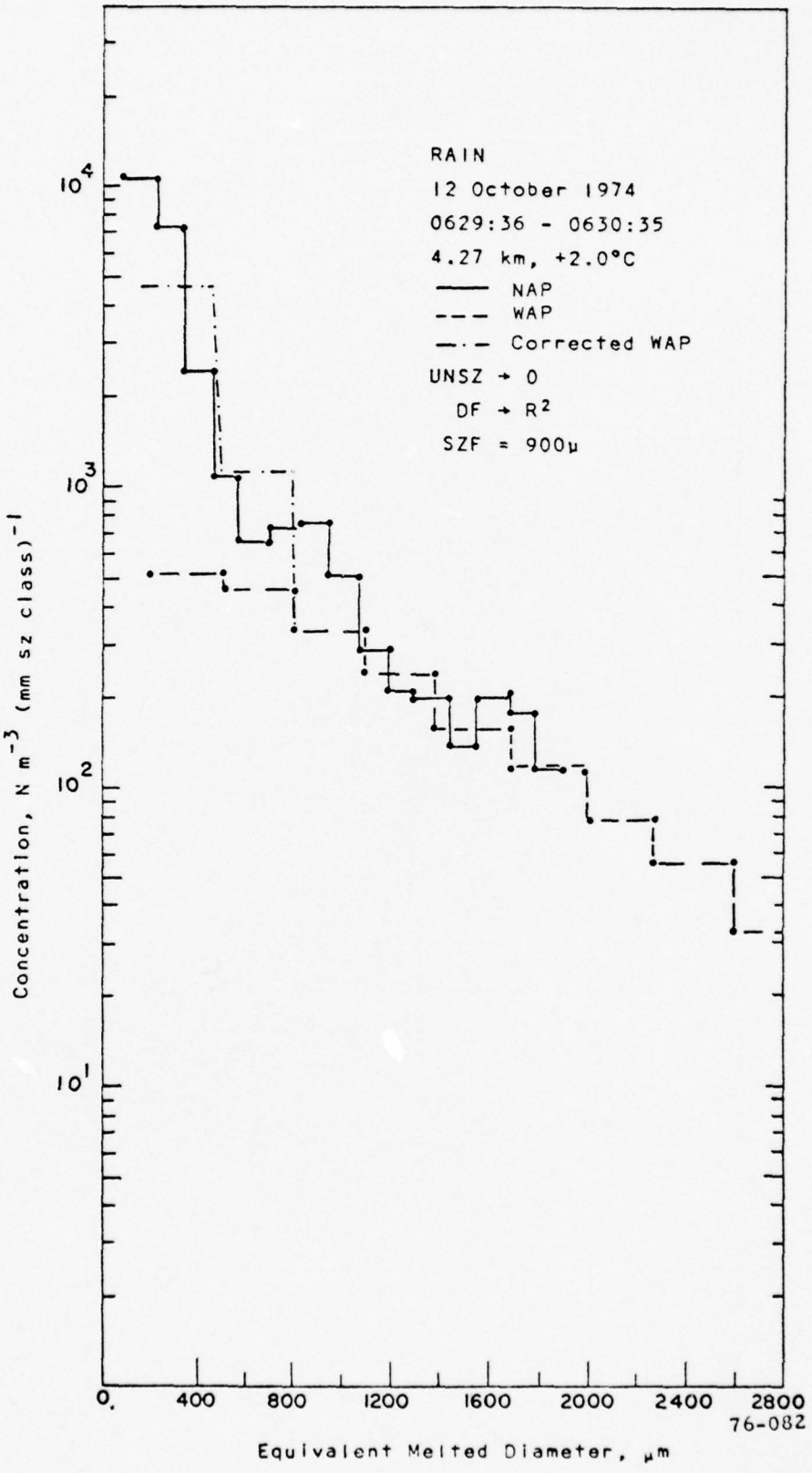

Figure 6. Comparative rain spectra and corrections as indicated in legend

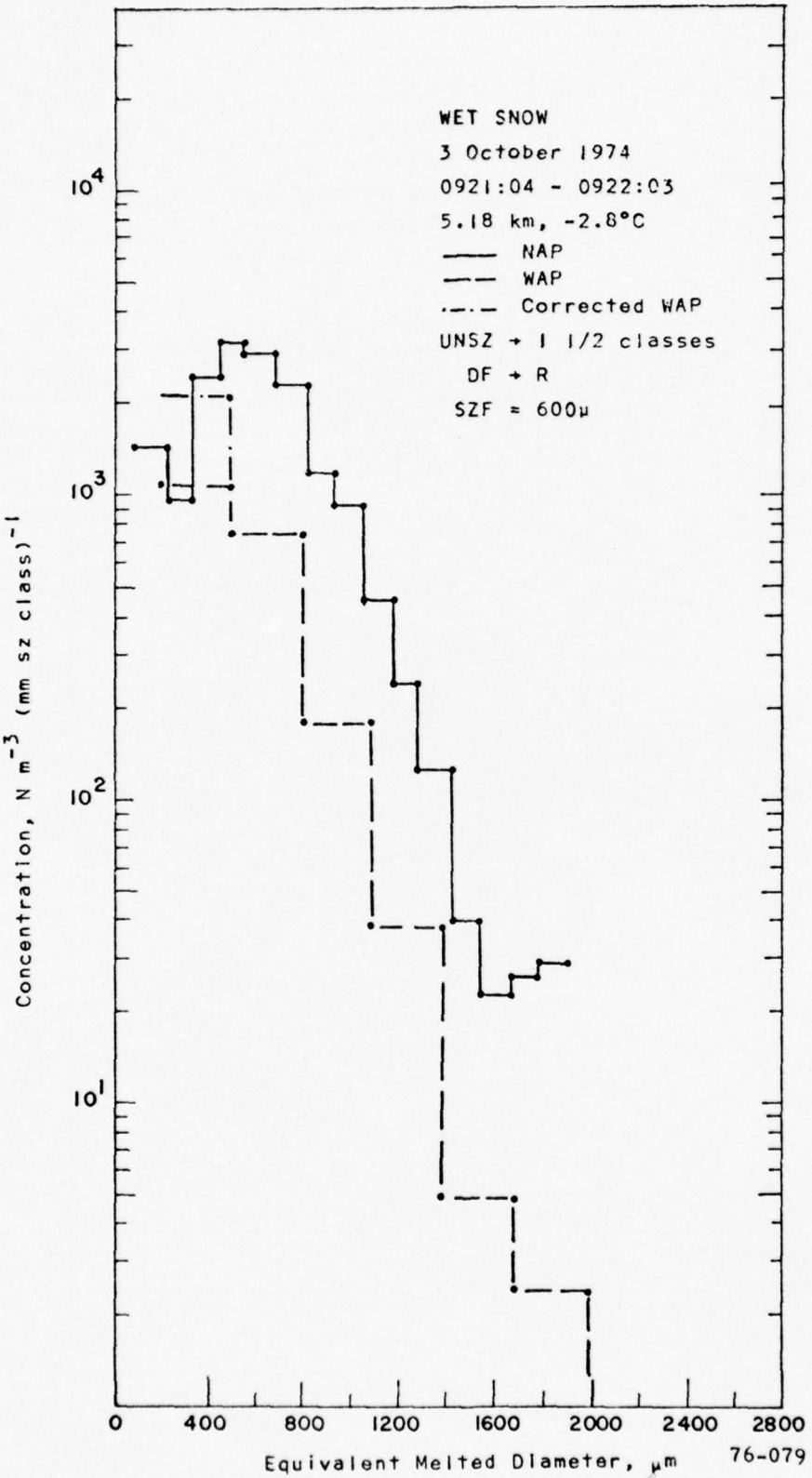

Figure 7. Comparative wet snow spectra with corrections as indicated in legend

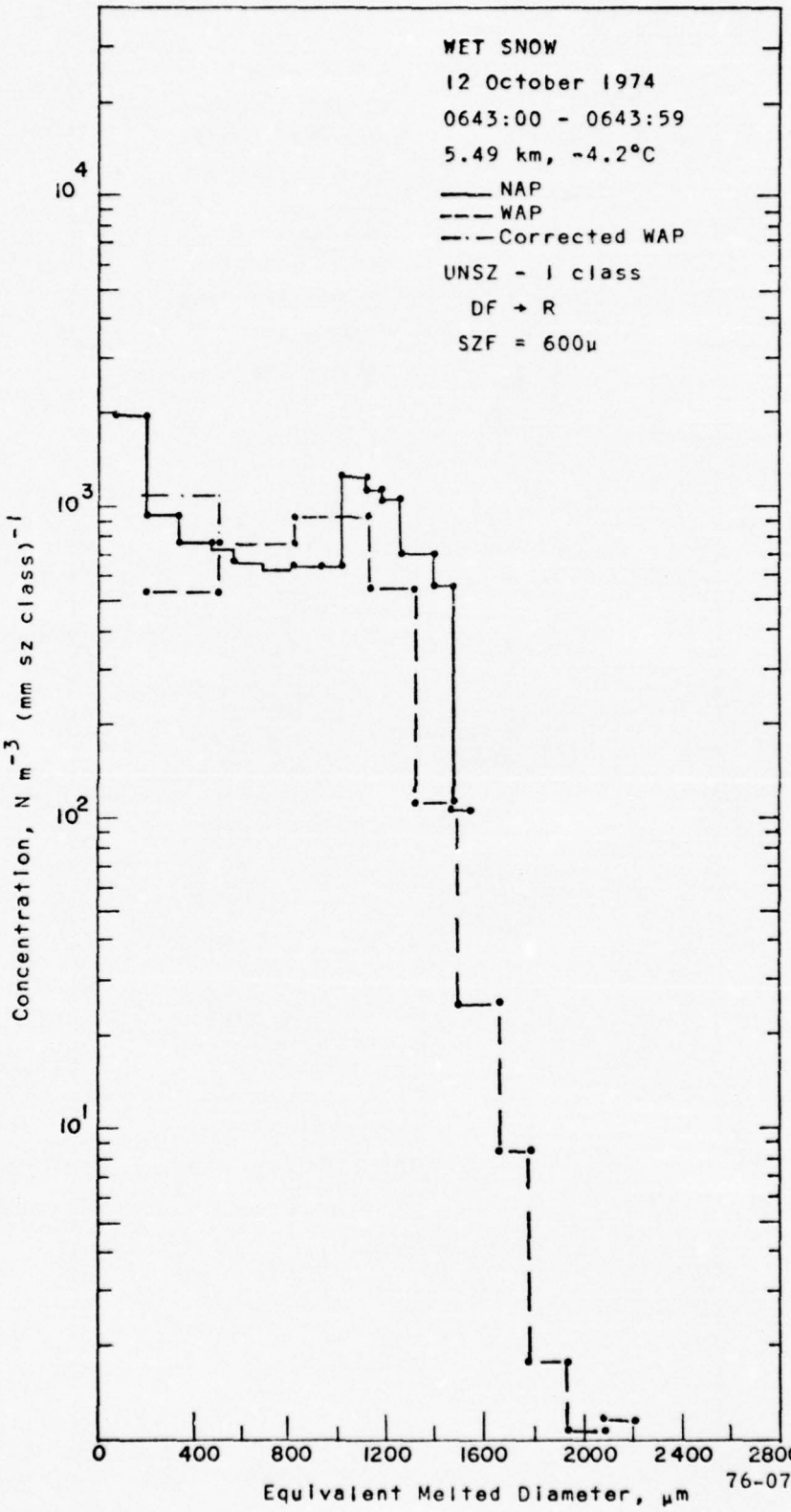

Figure 8. Comparative wet snow spectra with corrections as indicated in legend

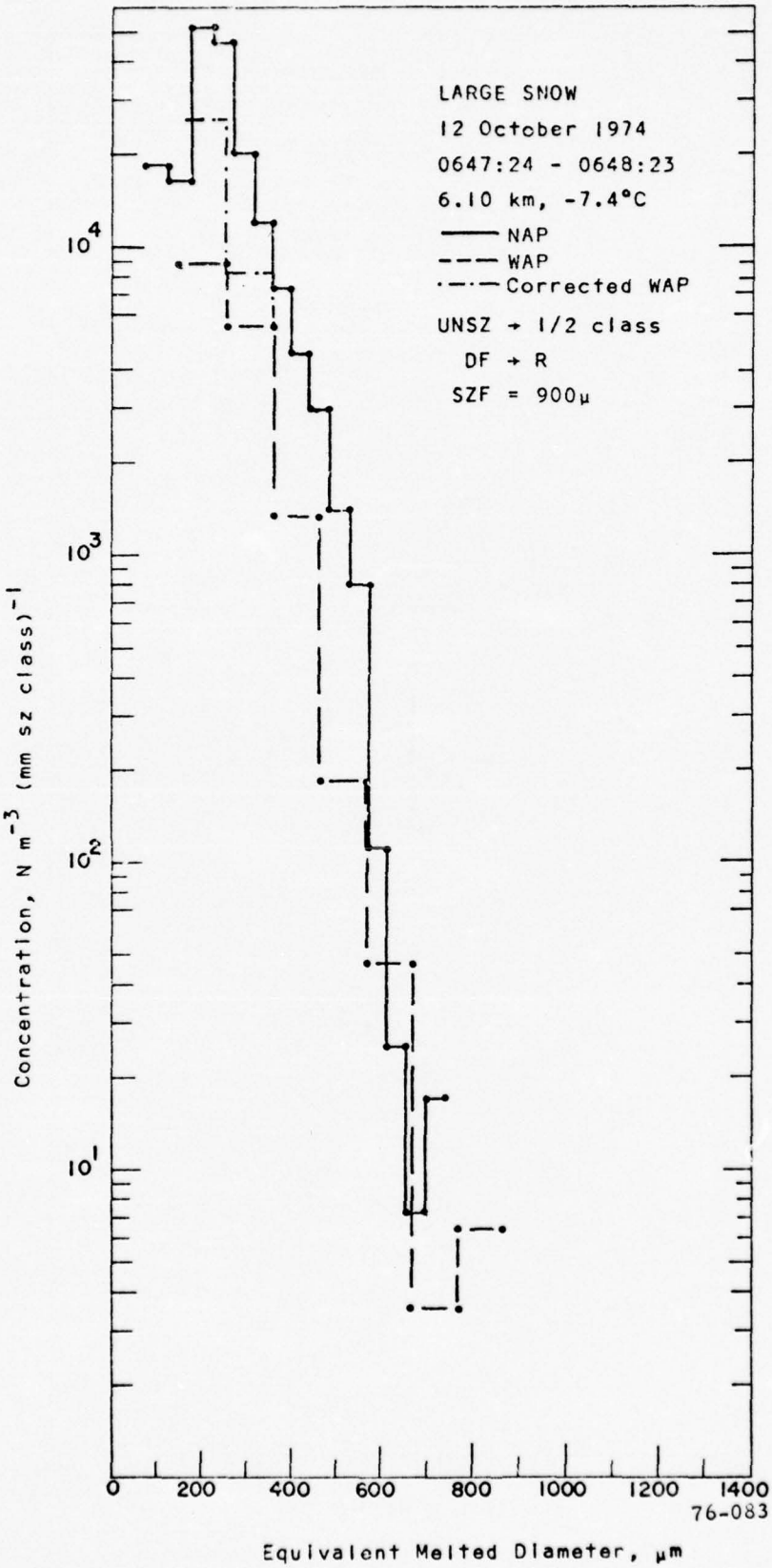

Figure 9. Comparative large snow spectra and corrections as indicated in legend

Figures 10 and 11 are illustrations of bullet rosettes and small snow spectra, respectively. Both spectra are exponential with only the UNSZ problem present. The approximate undersizing is two size classes (600 μm). No DF corrections were needed. The slopes of the NAP and WAP spectra were similar.

From this small sample of spectra it would appear that the problems and corresponding corrections are habit dependent. The R^2 dependence for the rain spectra and R for large snow suggest that depth of field depends upon the particle shape, being length squared for a spherical particle, and length for at least some snow particles. The bullet rosettes and the small snow do not show a DF problem. The problem is likely to be present in the first two size classes, however, undersizing eliminates these sizes, thus eliminating the depth of field problem. The UNSZ problem seems to be more severe for smaller snow particles (small snow and bullet rosettes) generally about two size classes. The undersizing gets smaller towards larger snow particle habits and disappears completely for rain. The above discussion is based only on a small sample. These results should be considered somewhat speculative at this time.

4.2 Water Content and Radar Reflectivity Factor. Calculations and Comparison Between the Two Probes

The WC and Z were calculated using the AFGL processed particle spectra. The equations used are described in detail by Heymsfield (1975a). They are:

$$m = \sum_{i}^{n} \frac{\pi}{6} d_{mi} N_i \quad [g\ m^{-3}] \tag{3}$$

$$Z = \sum_{i}^{n} N_i d^6_{mi} \quad [mm^6\ m^{-3}] \tag{4}$$

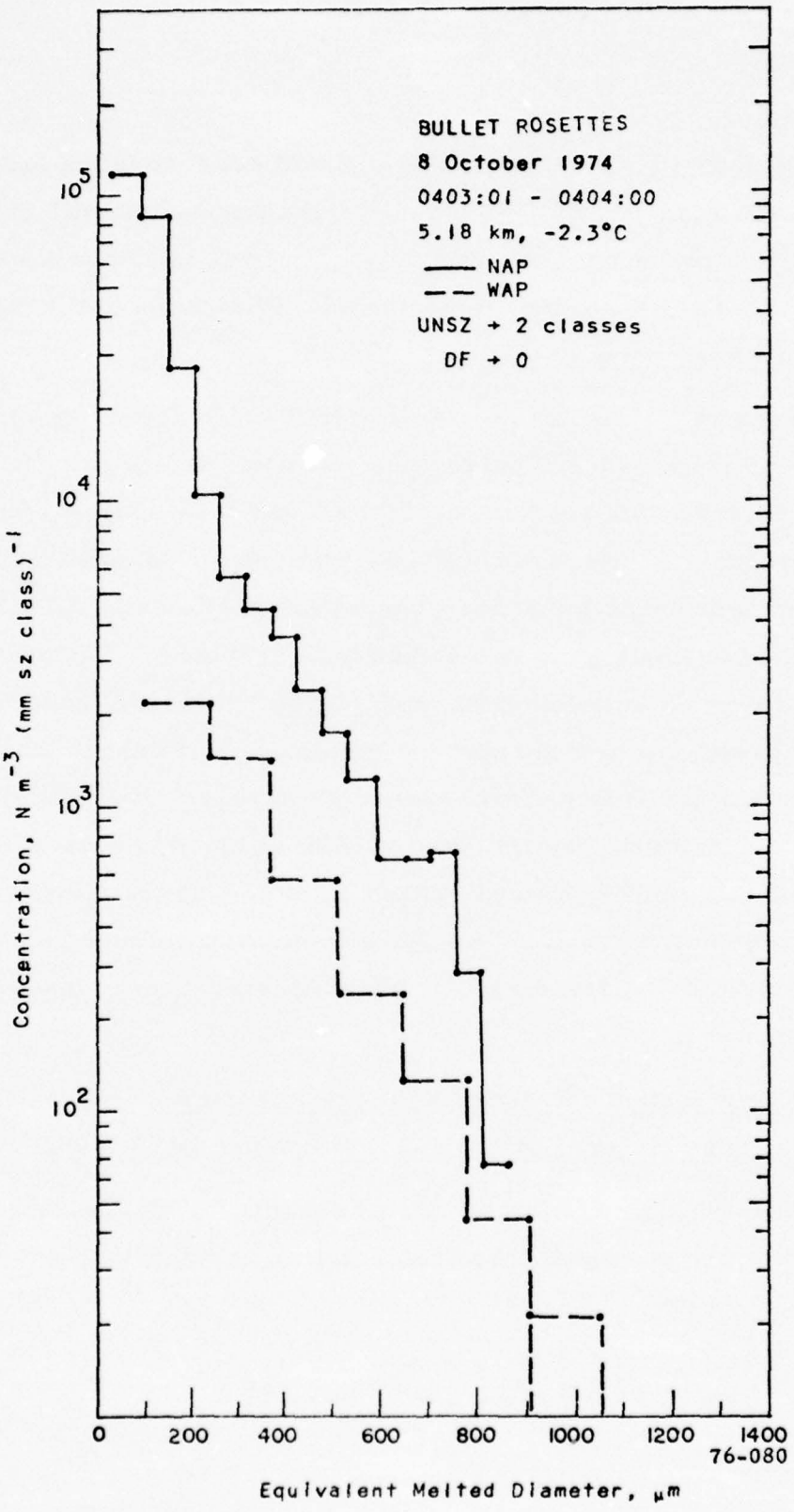

Figure 10. Comparative bullet rosette spectra and corrections as indicated in legend

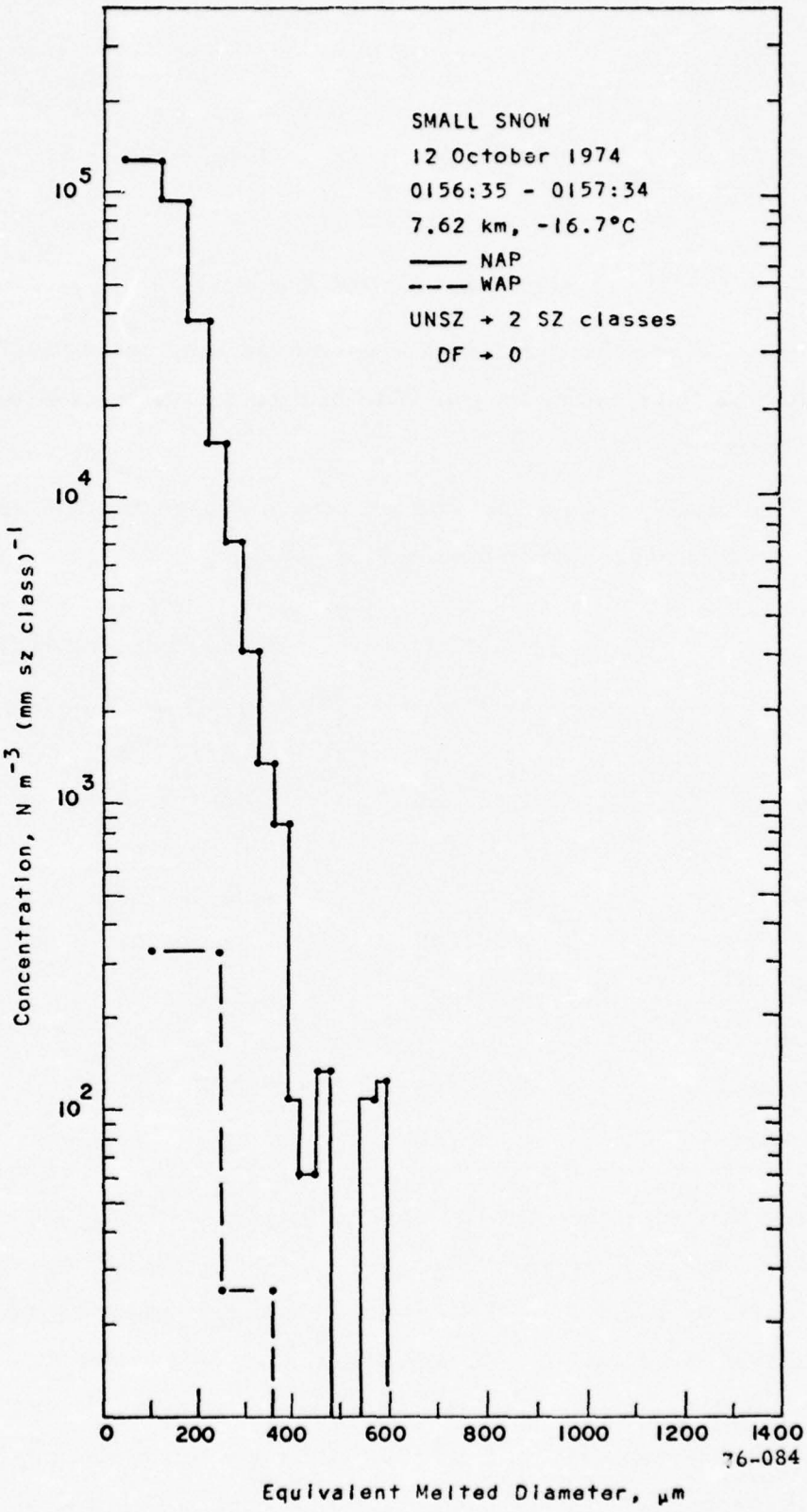

Figure 11. Comparative small snow spectra and corrections as indicated in legend

where $d_{mi} = a(SZ_i)^b$ and $SZ_i = R\,(X + YI)$

m = WC in g m^{-3}

d_m = equivalent melted diameter

a and b are the coefficient and the exponent, respectively, for changing a size length, SZ, into an equivalent melted diameter.

The following table lists the a's and b's used for WC and Z for the spectra presented in the previous section.

Type	Breakpoint (mm)	Equivalent Melted Diameter a	b
Rain	0.00	1.000E + 00	1.000
Wet snow	L < 1.00	1.000E + 00	1.000
Wet snow	L > 1.00	1.000E + 00	0.653
Large snow	L < 1.00	4.000E - 01	0.782
Large snow	L > 1.00	4.000E - 01	0.875
Small snow	L < 0.50	4.000E - 01	0.782
Small snow	L > 0.50	3.700E - 01	0.670
Bullet-rosettes	L < 0.20	2.560E - 01	0.667
Bullet-rosettes	L > 0.20	4.380E - 01	1.000

It is obvious that the corrected spectra resulted in values of WC and Z quite close to the NAP values. The corrections on the rain spectra, (spectra suffering from DF only) result in an improvement of the calculated values by 30 percent in WC and less than 1 dBZ in the calculated reflectivity factor. On the other hand, the corrections on the bullet rosettes and small snow spectra (spectra suffering a two size class shift) result in a much greater improvement: 80 percent in WC and more than

15 dBZ. The above observation points to the conclusion that undersizing in the WAP spectra is a more severe error than an undercounting of the small particles when WC and Z are the quantities of interest. The corrections presented in the previous section were only approximate, but the results of the calculations given in Table 2 show that these approximations essentially brought the probes into agreement.

5. COMPARISON OF AIRCRAFT AND RADAR MEASUREMENTS

5.1 Original Data Comparison

Pass-averaged aircraft calculations and radar reflectivity factor measurements, both processed by AFGL, appear in Figure 12. Note the agreement between radar measurements and the calculations of the NAP data at the upper two levels. There is approximately 2 dBZ difference between NAP data and radar, and 16-24 dBZ between WAP data and radar measurements. The next level shows a much lower radar reflectivity factor value for both aircraft probes, while the radar indicates a 6 dBZ increase. The crystal habit assumed in the data processing of this level was dendrites. In the next two levels, the calculated reflectivity factor values are 14 and 23 dBZ higher, respectively, than the radar measured values; data processing assumed wet snow for the 5.8 km level and rain for the 4.8 km level.

Little change in reflectivity factor results from the application of the current Knollenberg correction factors. Figure 13 illustrates the change.

The strong disagreement of the lower three levels can be explained largely on the basis of incorrect choice of crystal habit or hydrometeor phase. It should be reiterated that no replicator data were available. The predominant crystal habit should have been bullet rosettes, at the lower three levels, for the following reasons:

TABLE 2. SUMMARY OF THE CORRECTIONS AND CALCULATIONS PERFORMED ON THE PRECEDING SPECTRA*

1974	WAP Errors		WC			dBZ		
	UNSZ (Size classes shift)	DF (SZF)	NAP	WAP		NAP	WAP	
				Uncorrected	Corrected		Uncorrected	Corrected
Rain								
October 2	0	R^a (1200 μm)	0.074	0.038	0.053	24.5	22.8	22.8
October 12	0	R^a (900 μm)	0.448	0.347	0.413	34.3	33.7	34.0
Wet Snow								
October 3	1.0	R (600 μm)	0.375	0.077	0.374	27.6	20.1	28.4
October 12	0.5	R (600 μm)	0.589	0.338	0.495	32.6	29.1	31.6
Large Snow								
October 12	1.0	R (900 μm)	0.310	0.053	0.242	16.2	7.5	15.2
Bullet Rosette								
October 8	2.0	0	0.200	0.033	0.154	17.5	10.0	20.4
Small Snow								
October 12	2.0	0	0.073	3.4×10^{-4}	0.003	5.4	-20.5	-3.0

*Figures 5-11, incl.

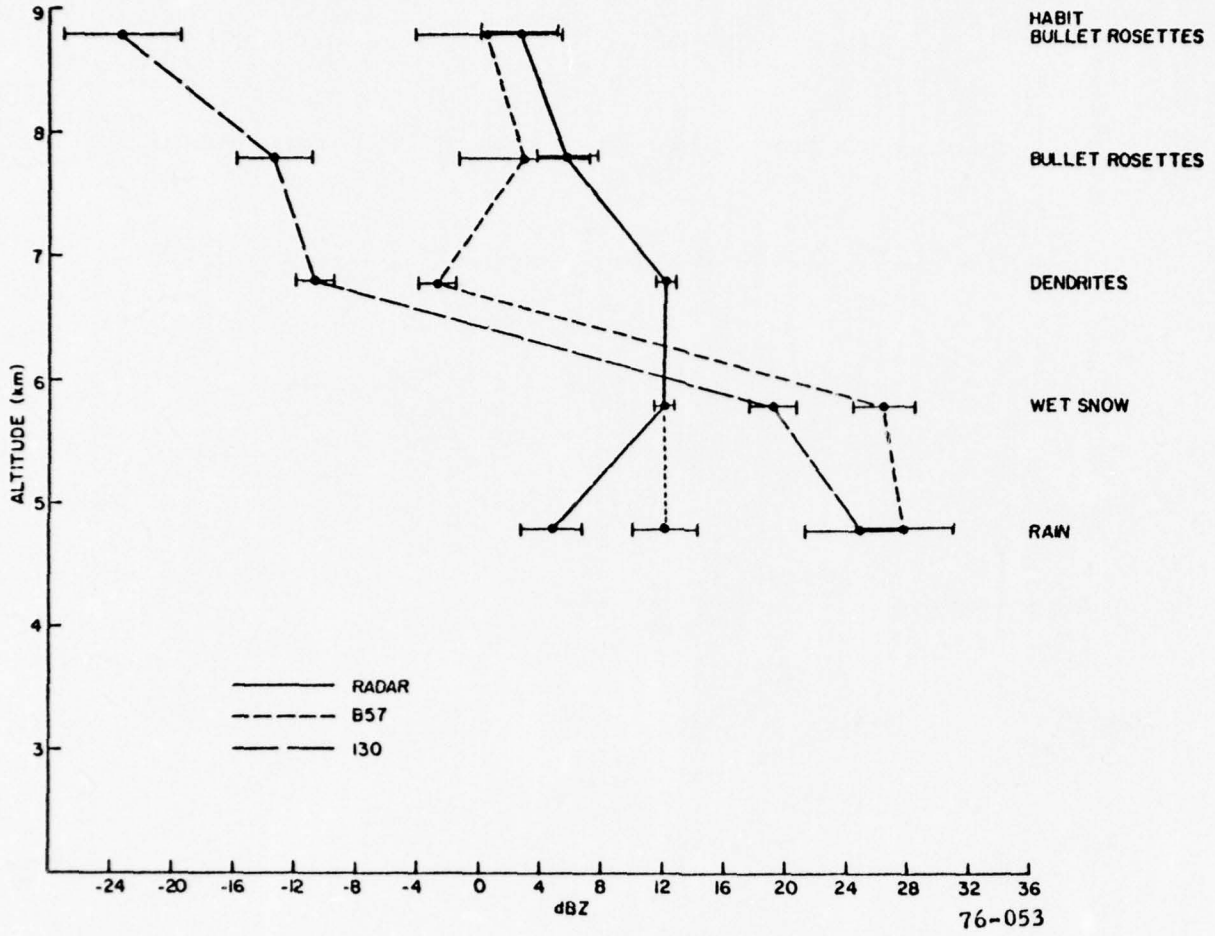

Figure 12. Pass-averaged dBZ (calculated from NAP and WAP probes and measured by radar) as originally processed

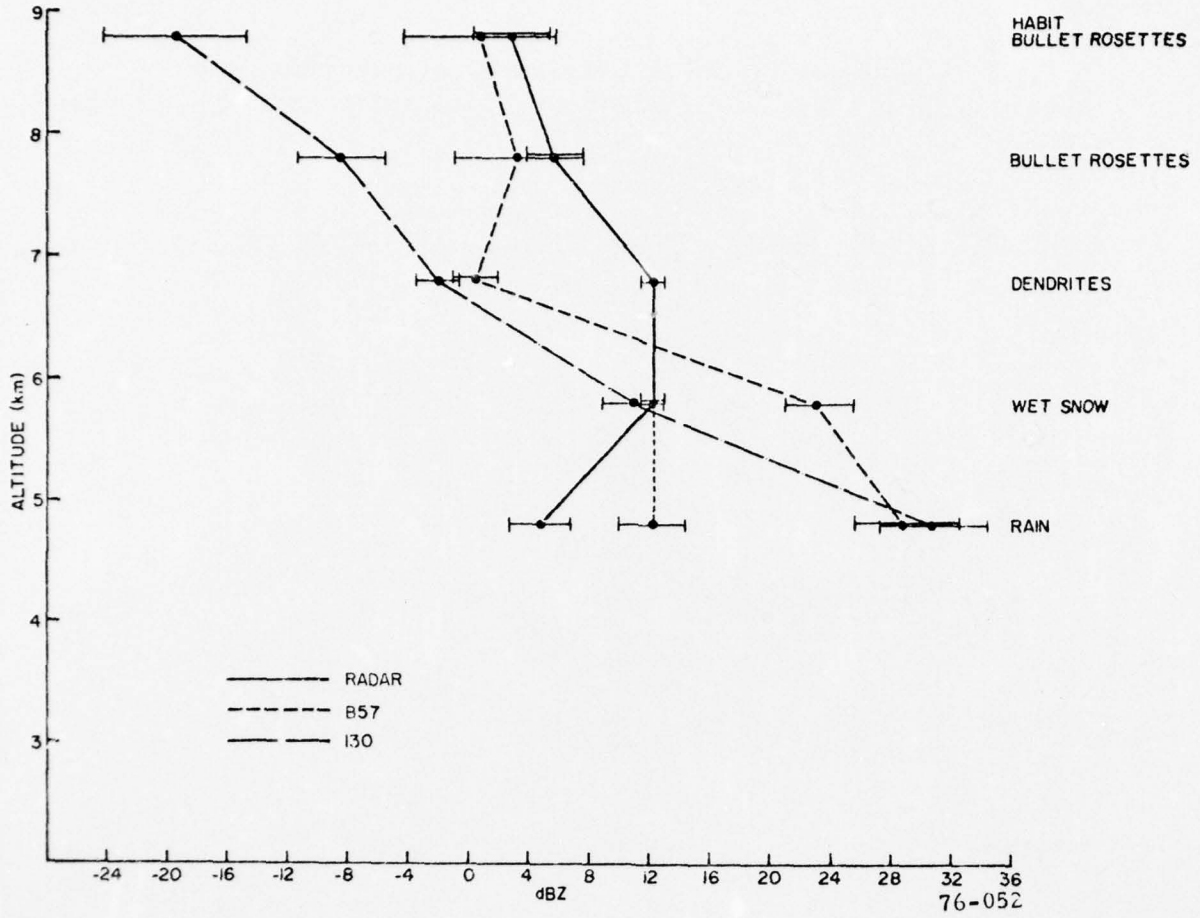

Figure 13. Same as Figure 12 with Knollenberg corrections

1. The aircraft observer reported a 22-1/2° halo throughout the entire cloud. This observation is indicative either of columnar or bullet rosette ice particles.

2. No significant growth of particle size took place between 7.8 and 4.8 km, as evidenced by the nearly constant value of Z between these levels.

3. Particle spectra at 5.8 and 4.8 km were nearly identical in form and total number concentrations. Clearly, virtually no melting could have taken place at the 4.8 km level, and some type of aggregate ice particle would be a more correct choice.

5.2 Corrected Results

Figure 14 illustrates changes in the reflectivity factor in the lower three levels due to correction of particle habit. The habit selected for the purposes of these calculations was bullet rosettes. Considerably better agreement for both probes at these levels indicates that the choice of bullet rosettes was a more appropriate particle habit. The WAP results are only 7 dBZ lower than the radar measurements at 6.8 km compared to a 14 dBZ difference before the habit type was changed. The NAP data results in consistently lower reflectivity factors than measured by the radar. This can be attributed to the truncation of the particle spectrum at 1.8 mm -- an error which could have been improved by extrapolating the spectrum to larger sizes.

Figure 15 shows the improvement of the WAP results when corrected for the undersizing problem. The particle spectra (for 1-minute intervals at each level) during the ALCOR correlations are illustrated in Figures 16-20. Note how the only problem existing throughout is undersizing. This observation agrees with the previously concluded

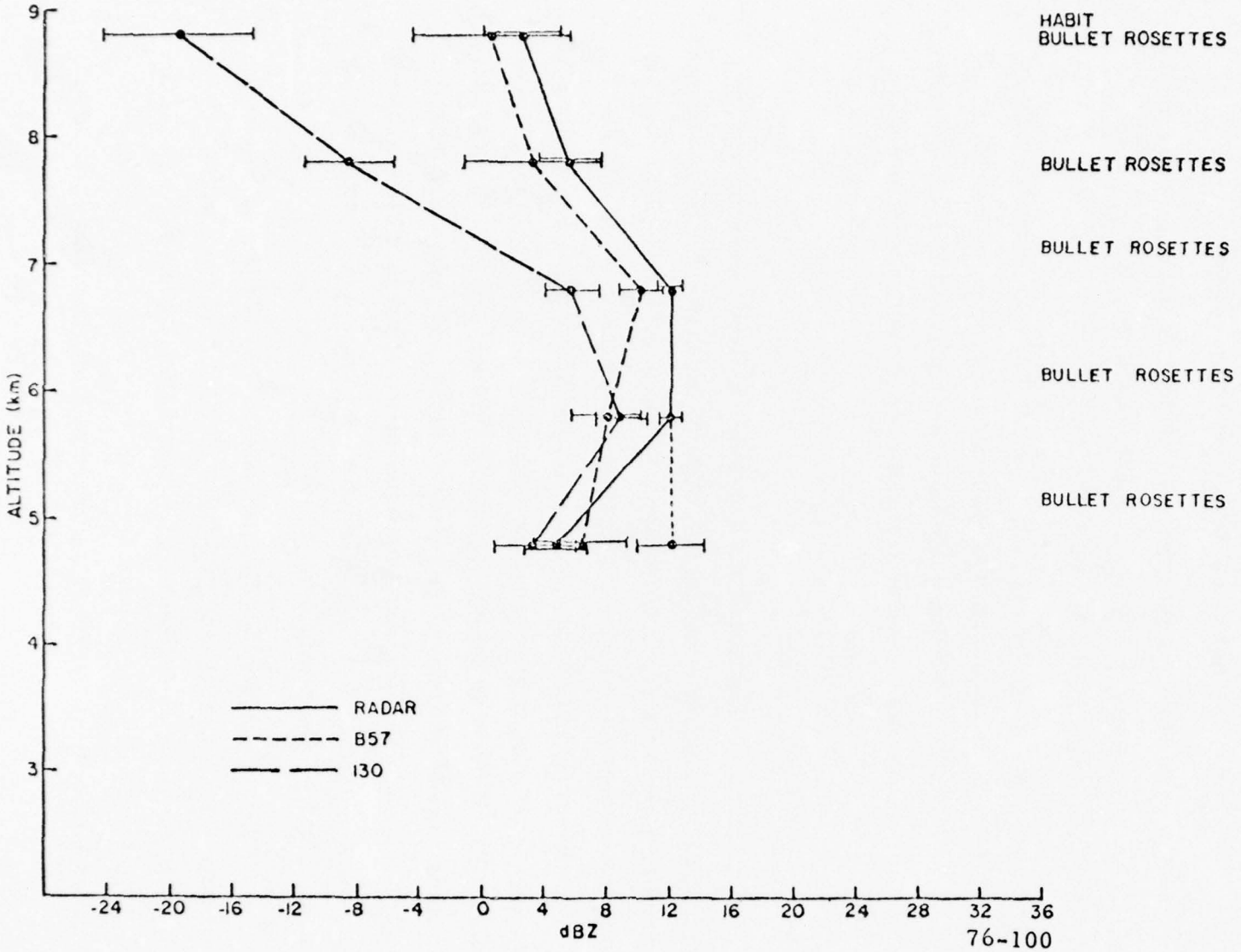

Figure 14. Same as Figure 13 with correction of particle habit in the lower three levels

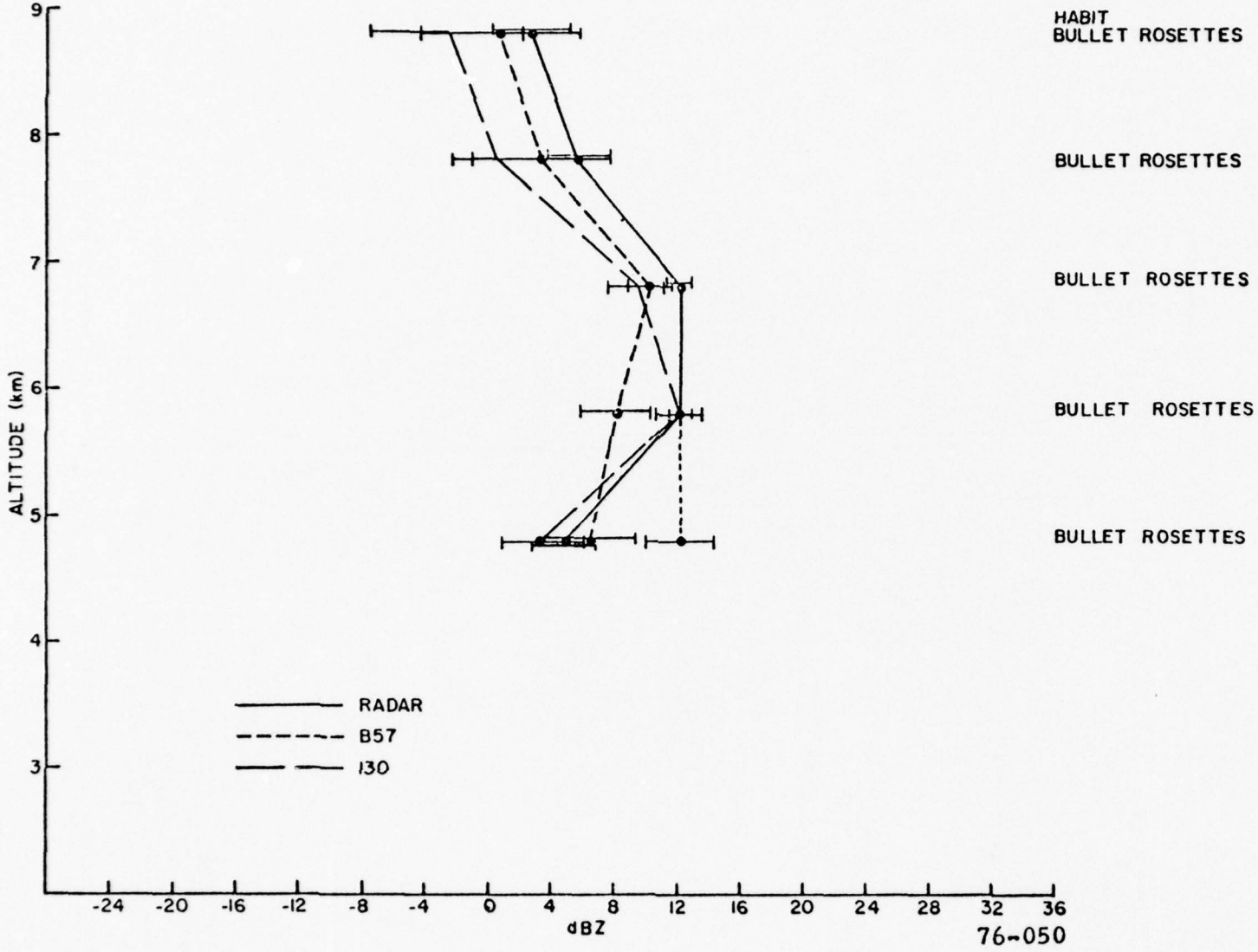

Figure 15. Same as Figure 14 with correction for UNSZ

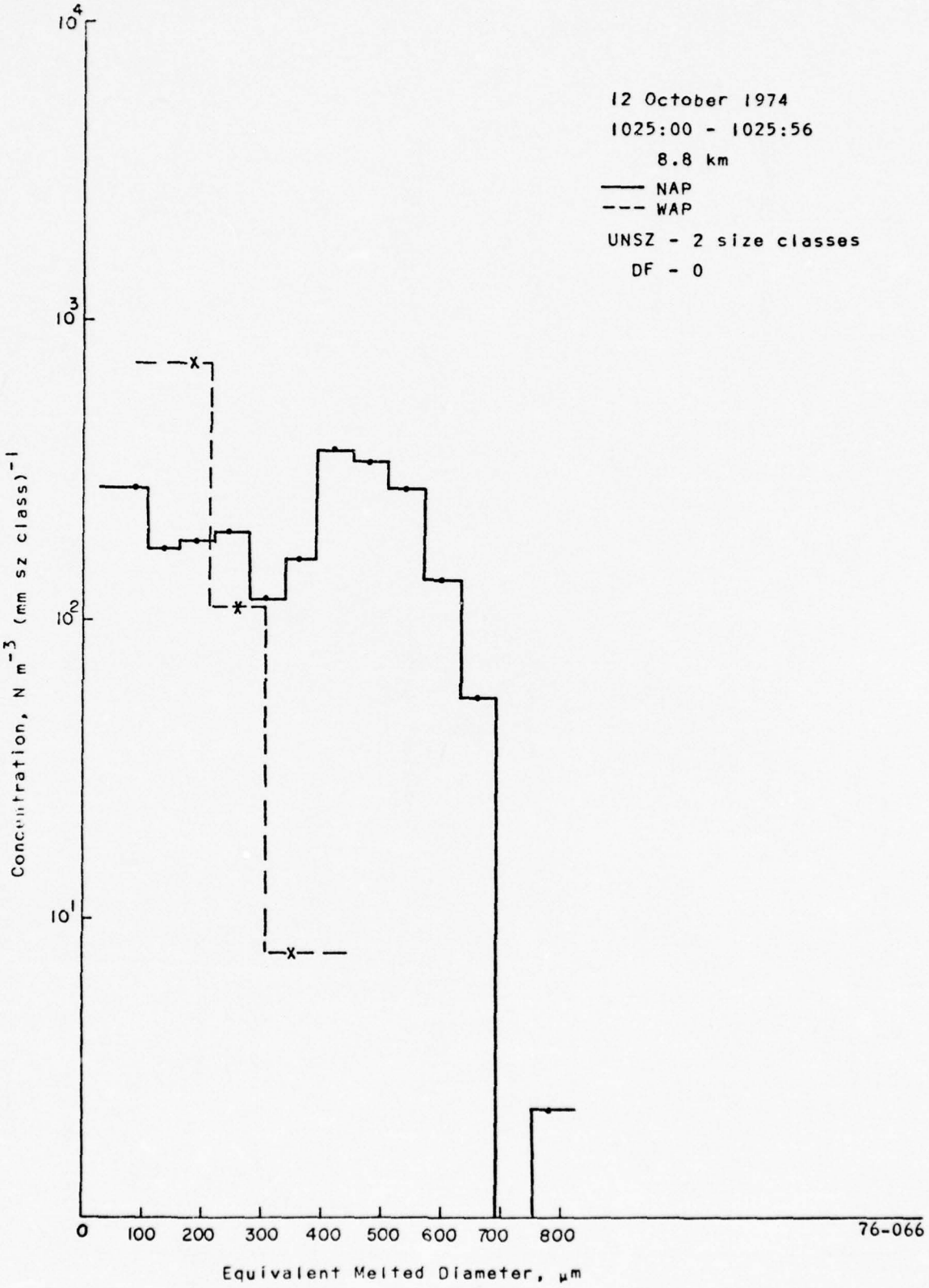

Figure 16. Comparative particle spectra during ALCOR radar correlation. See legend and text for explanation.

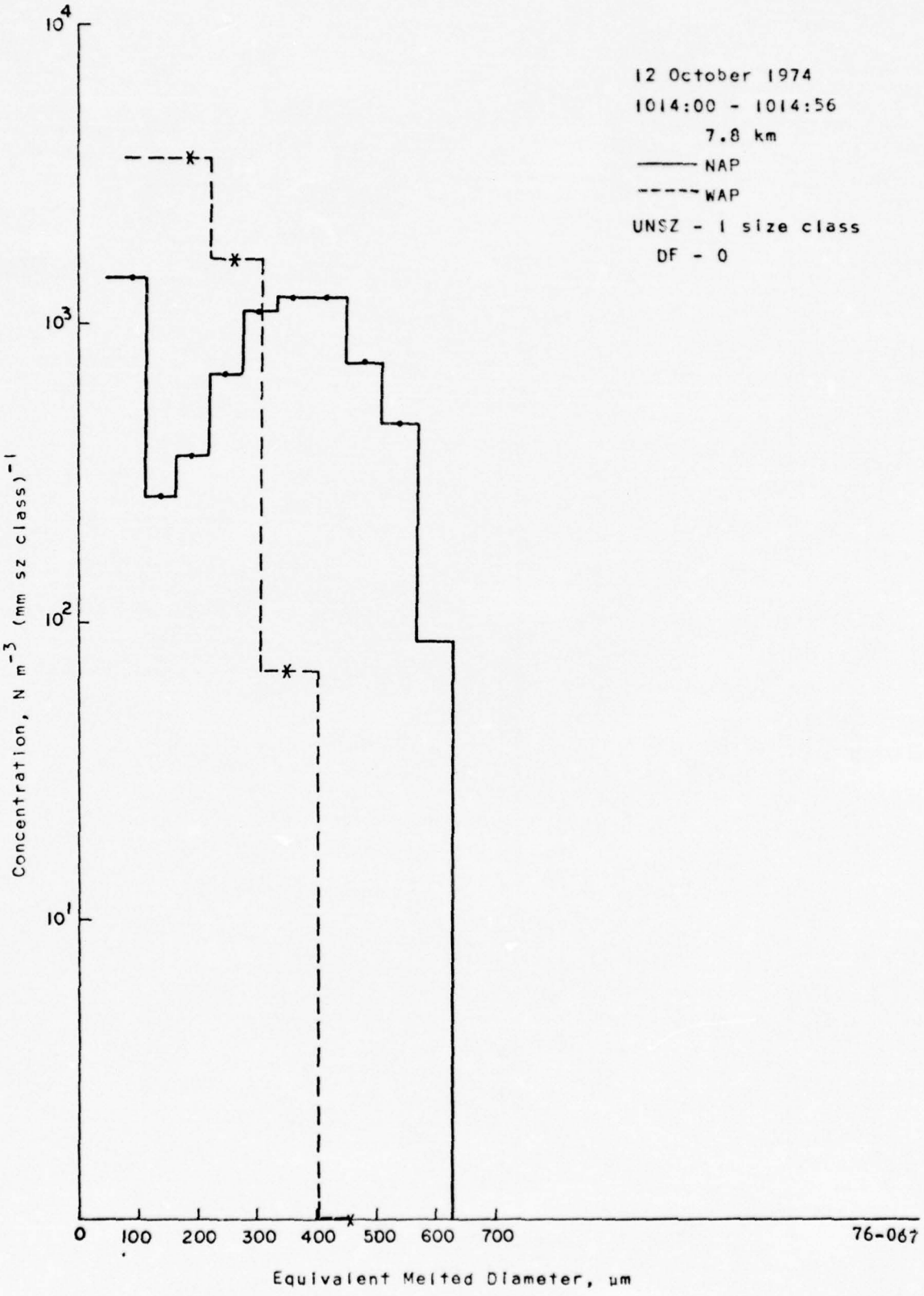

Figure 17. Comparative particle spectra during ALCOR radar correlation. See legend and text for explanation.

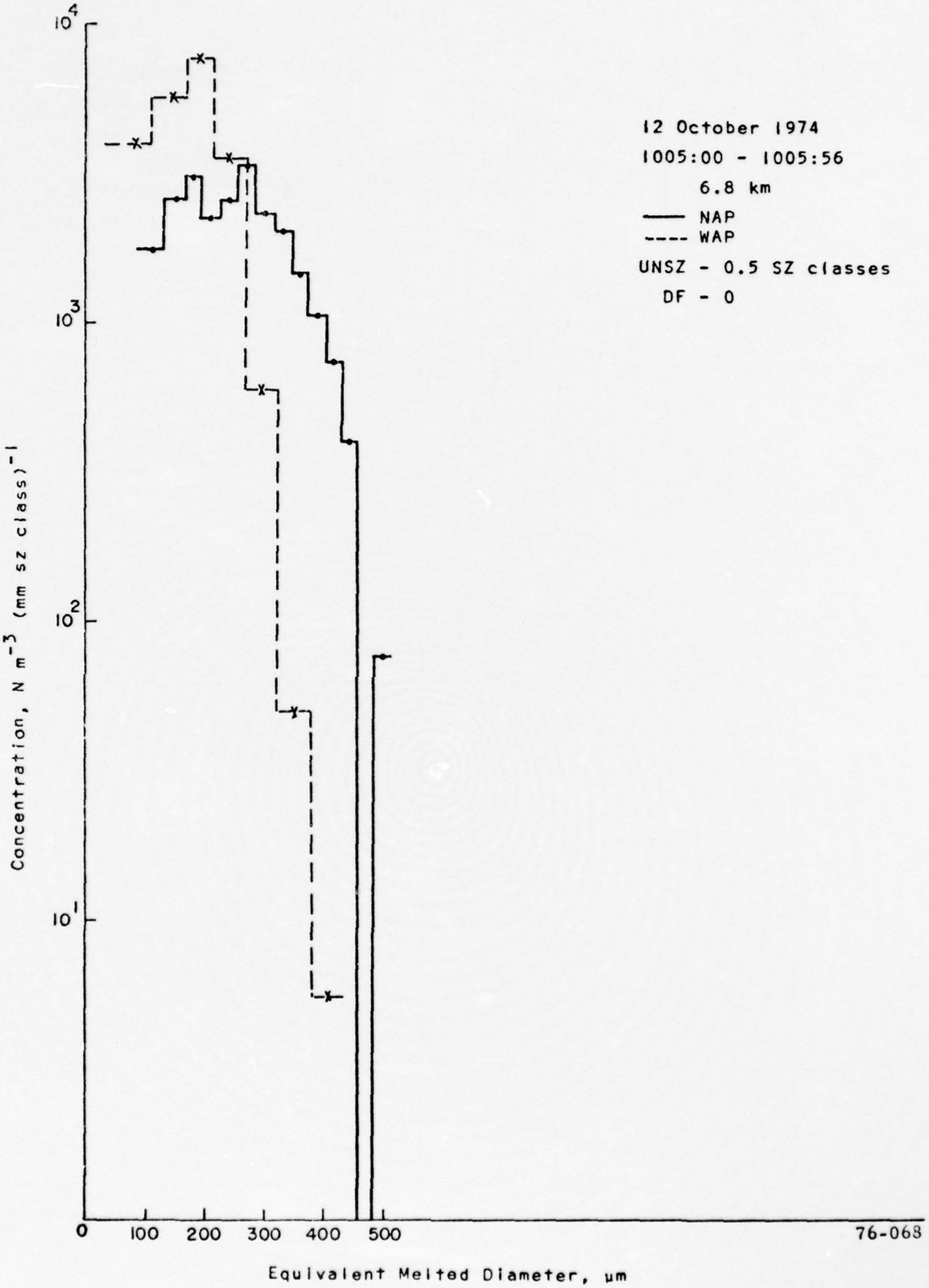

Figure 18. Comparative particle spectra during ALCOR radar correlation. See legend and text for explanation.

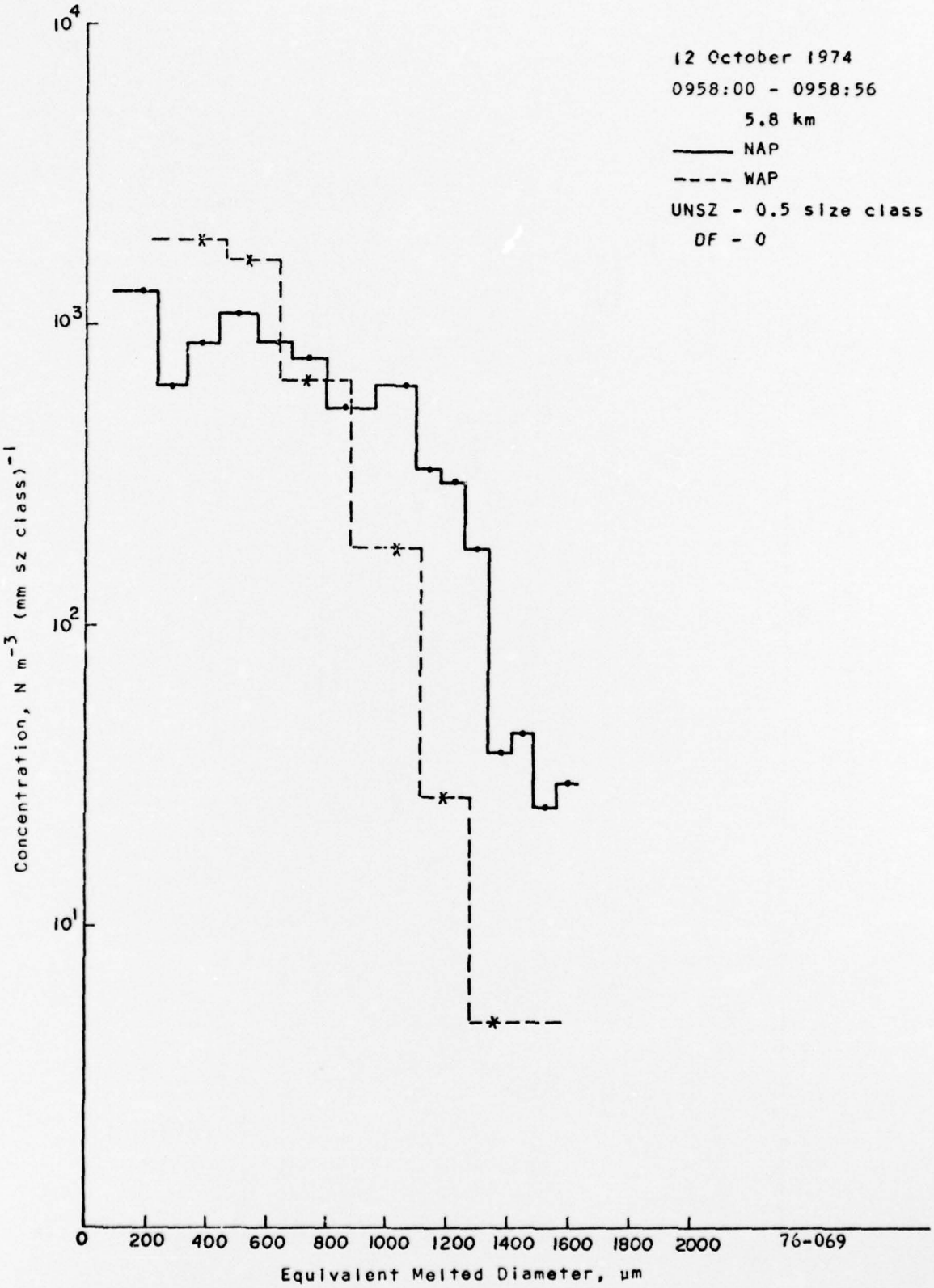

Figure 19. Comparative particle spectra during ALCOR radar correlation. See legend and text for explanation.

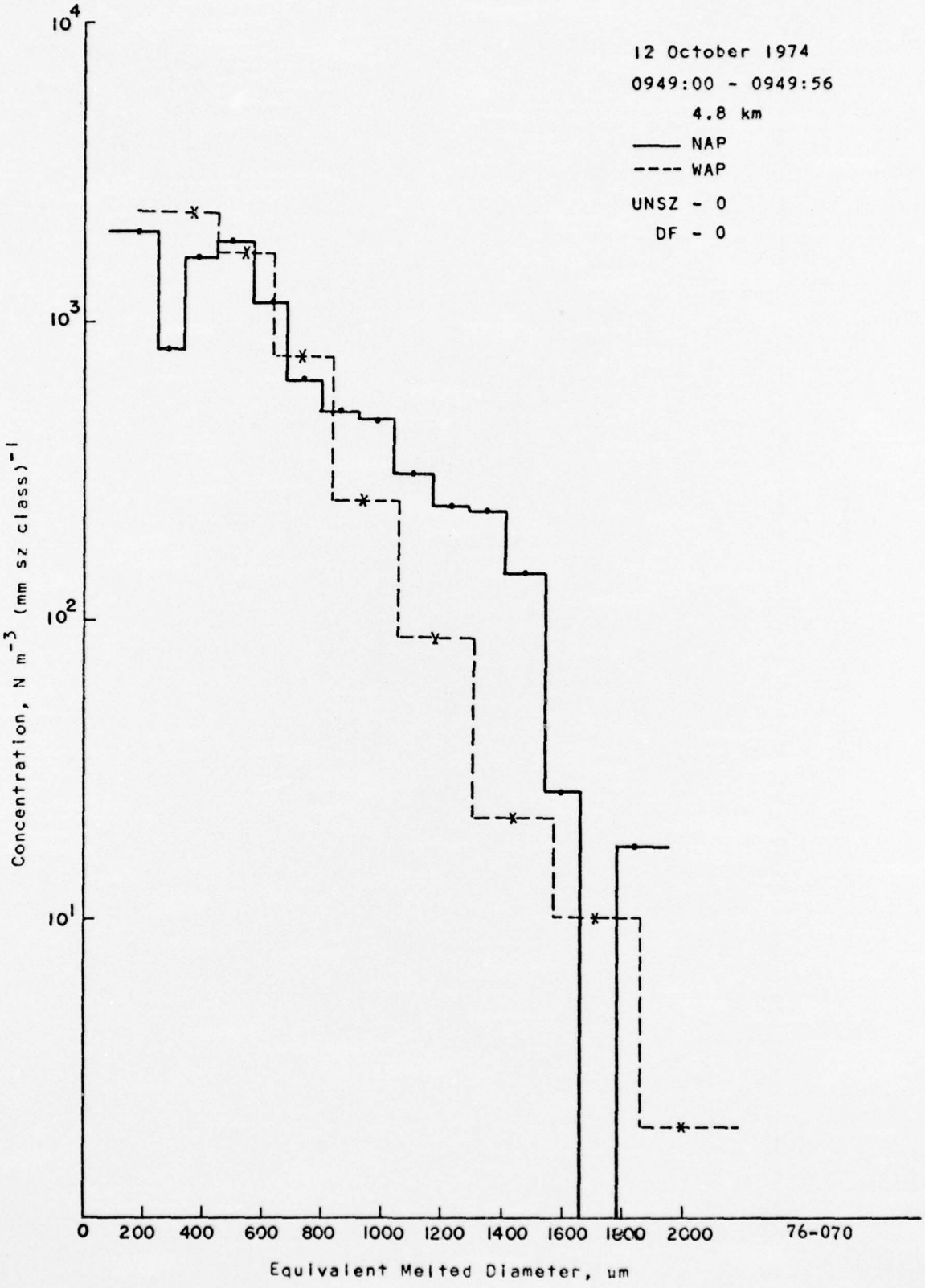

Figure 20. Comparative particle spectra during ALCOR radar correlation. See legend and text for explanation.

fact that WAP spectra of bullet rosettes suffer from only the UNSZ problem. The above observation is another strong argument for the change in habit type to bullet rosettes in the lower three layers of the run.

Table 3 summarizes the radar data and the aircraft calculation results for the different corrections applied. The final results are within 2 dBZ for the NAP data and 5 dBZ for the WAP data. These are small errors compared to the discrepancies that existed before the corrections (Kn, habit, UNSZ) were applied.

The radar reflectivity factor data processed in 8-second averages for both aircraft and radar are plotted in Figures 21-25. These figures illustrate the change of dBZ with time at a constant level in the cloud. The "uncorrected" and "corrected" aircraft results are plotted. Similar to the pass-averaged reflectivity factor graphs, the discrepancies between the radar data and aircraft calculations get smaller with each correction applied. A noticeable difference between the radar and aircraft curves is the smoothness of the radar measurements due to spatial averaging.

6. CONCLUSIONS

Systematic discrepancies in size spectra measurements between the two PMS probes were found. Corrections were applied to the WAP measurements, thereby, reducing the discrepancies between the two spectra. The correlation runs allowed the comparison between the results of the two probes and the radar data. Once Knollenberg corrections and the change to appropriate habit were performed, the NAP results were within 2 dBZ of the radar measurements. Two other corrections were developed for the WAP data: UNSZ (undersizing) and DF (undercounting). These corrections brought the wide-arm probe results within 5 dBZ of the radar measurements, which represents a 20 dBZ improvement from the initial 25 dBZ difference.

TABLE 3. COMPARISON OF MEASURED VS CALCULATED RADAR REFLECTIVITY FACTOR (dBZ) TASS, AVERAGED

Altitude (km)		8.8	7.8	6.8	5.8	4.8	
ALCOR (dBZ)		2.8	5.8	12.3	12.2	4.8	(12.2)
Habit Used In Calculation	initially	Bullet Rosettes	Bullet Rosettes	Dendrites	Wet Snow	Rain	(Ice)
	corrected	----------	Bullet Rosettes	----------			
NAP	uncorrected	0.5	2.9	- 2.7	26.4	27.8	
	Kn	0.7	3.3	0.4	23.2	29.0	
	habit	0.7	3.3	10.4	8.1		6.5
WAP	uncorrected	-23.4	-13.3	-10.7	19.2	24.6	
	Kn	-19.4	- 8.5	- 2.1	10.9	30.8	
	habit	-19.4	- 8.5	5.9	9.0		3.4
	UNSZ	- 2.5	0.6	9.3	12.1		3.4

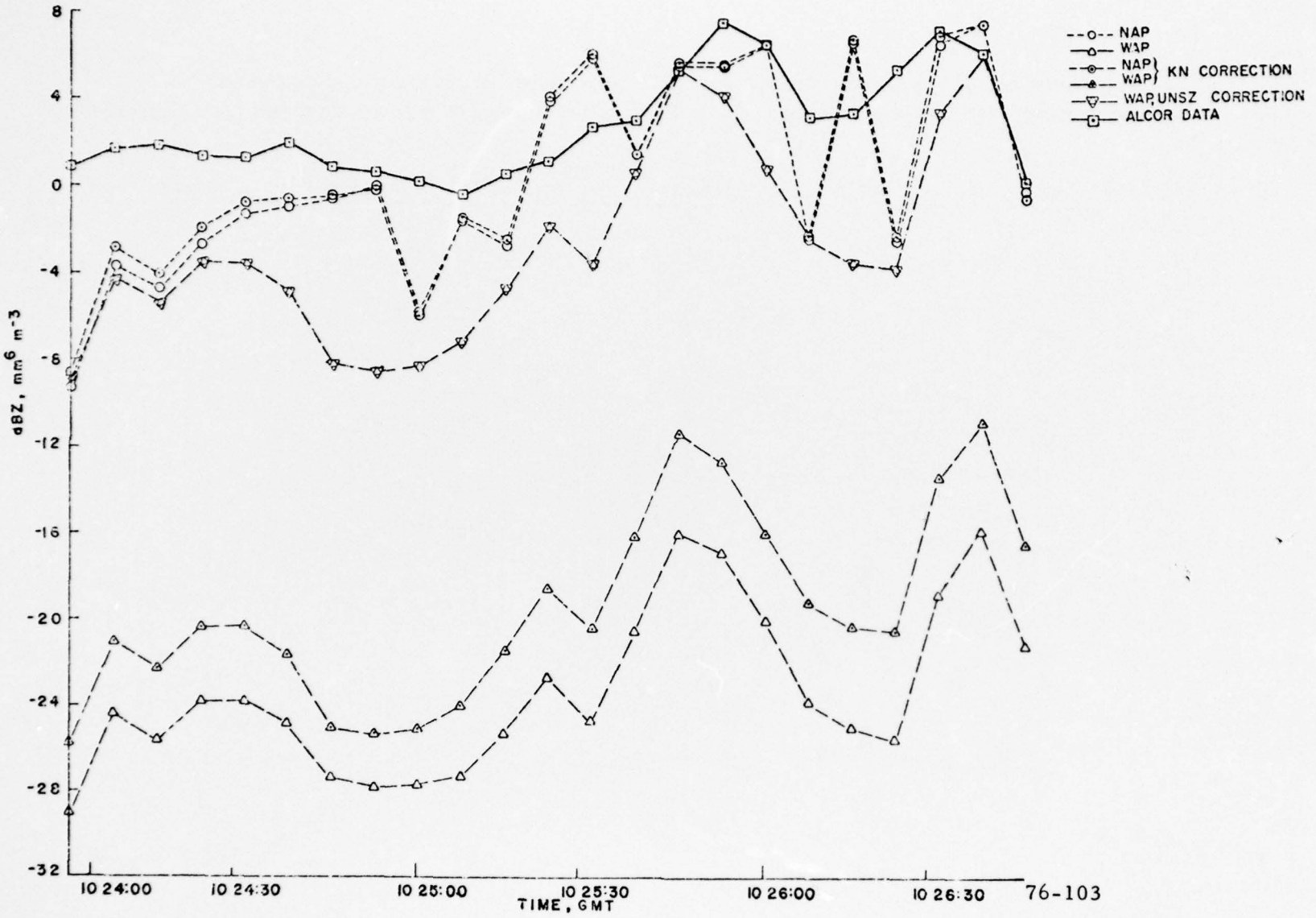

Figure 21. Time plots of dBZ in 8-second averages for radar and aircraft. Both original and corrected aircraft-calculated dBZ are shown. See legend for specifics.

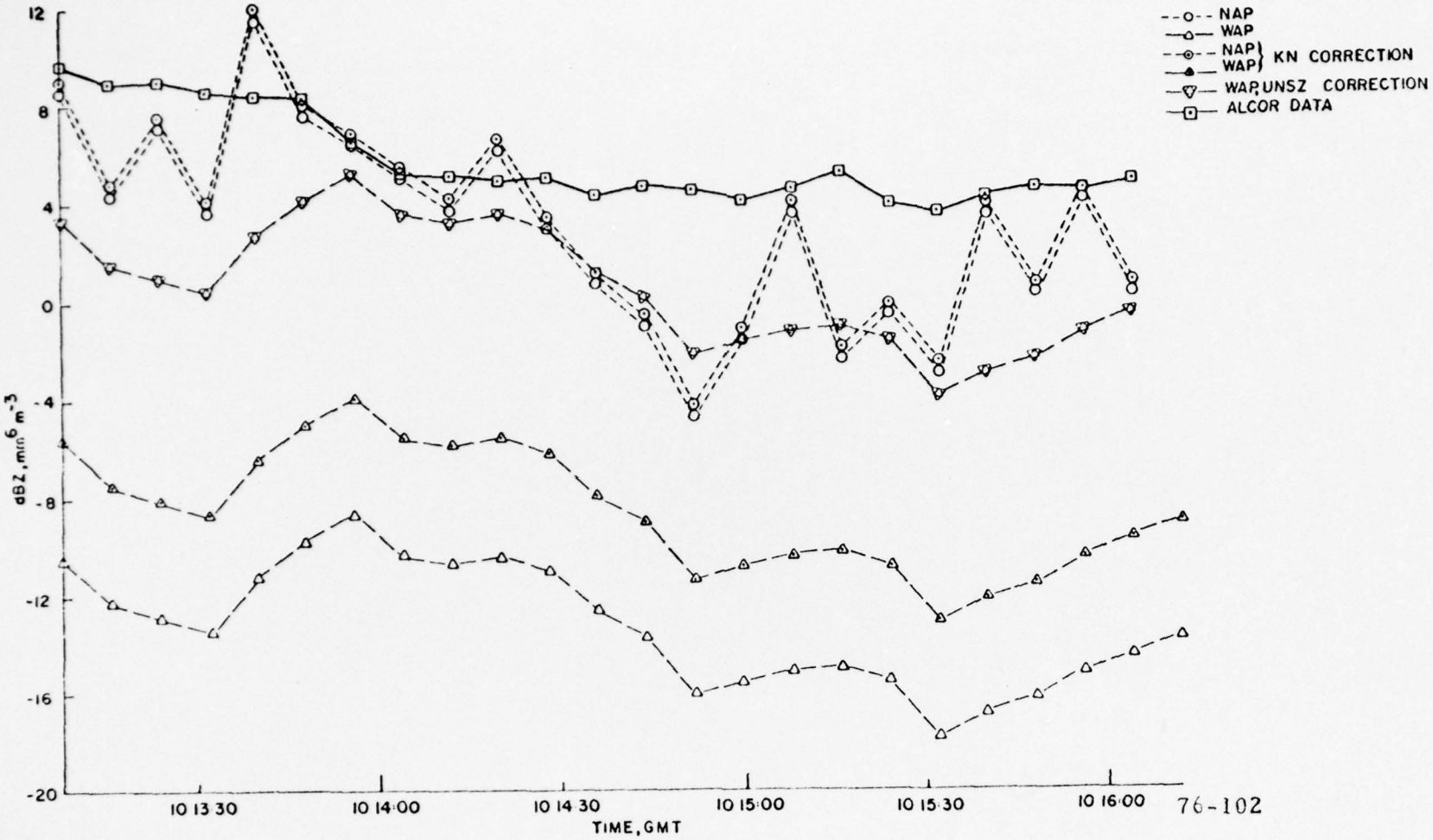

Figure 22. Time plots of dBZ in 8-second averages for radar and aircraft. Both original and corrected aircraft-calculated dBZ are shown. See legend for specifics.

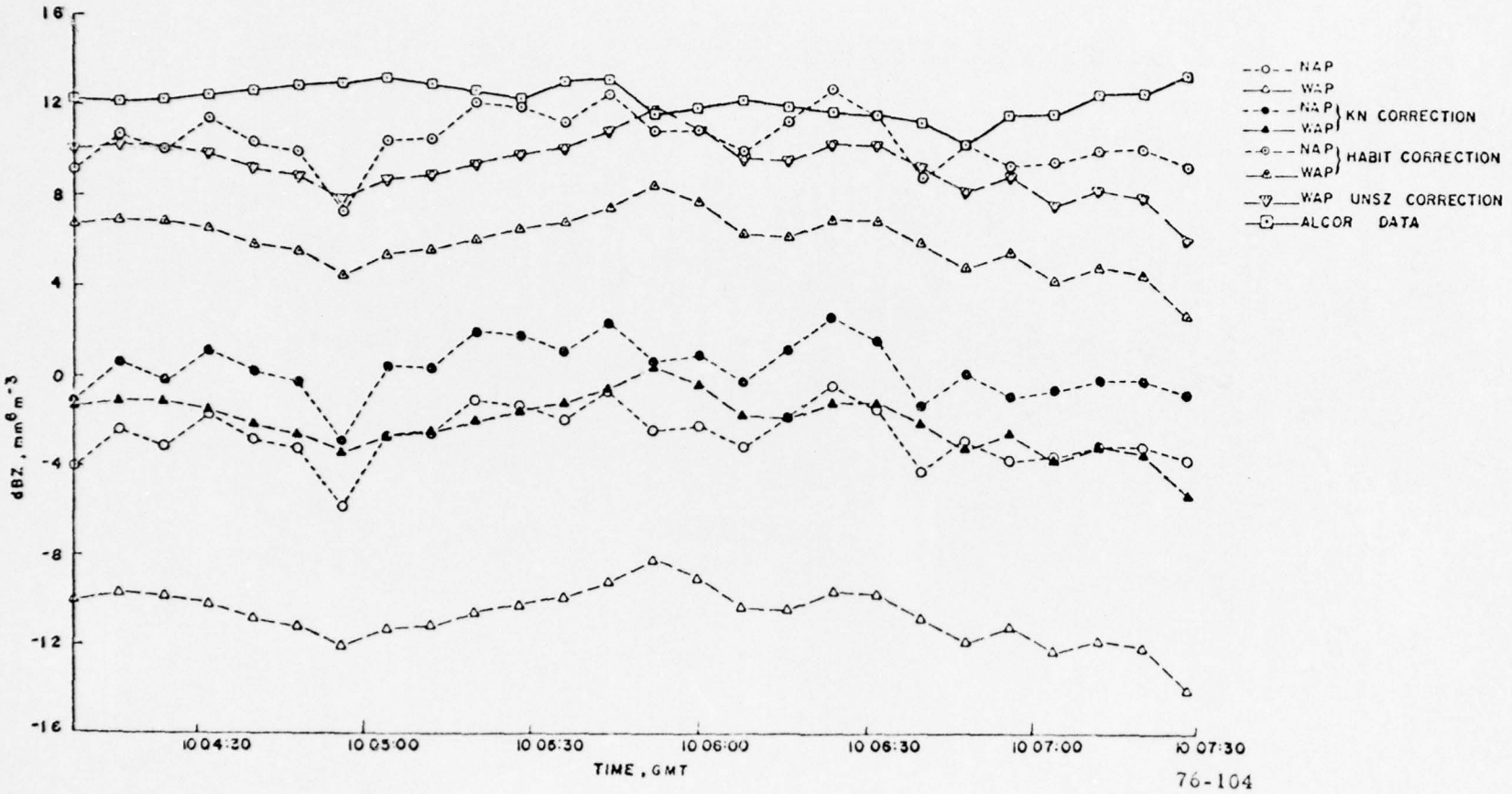

Figure 23. Time plots of dBZ in 8-second averages for radar and aircraft. Both original and corrected aircraft-calculated dBZ are shown. See legend for specifics.

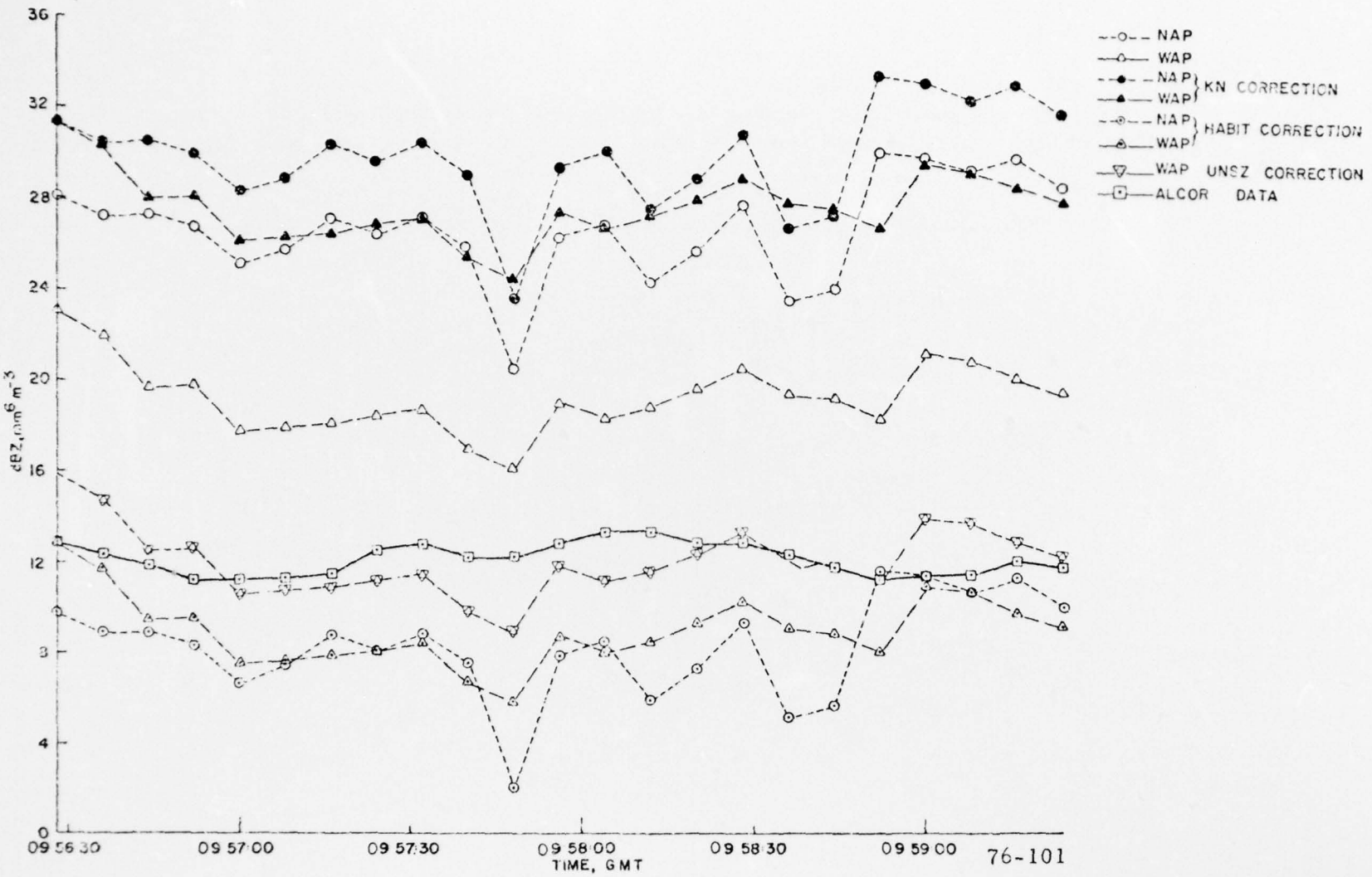

Figure 24. Time plots of dBZ in 8-second averages for radar and aircraft. Both original and corrected aircraft-calculated dBZ are shown. See legend for specifics.

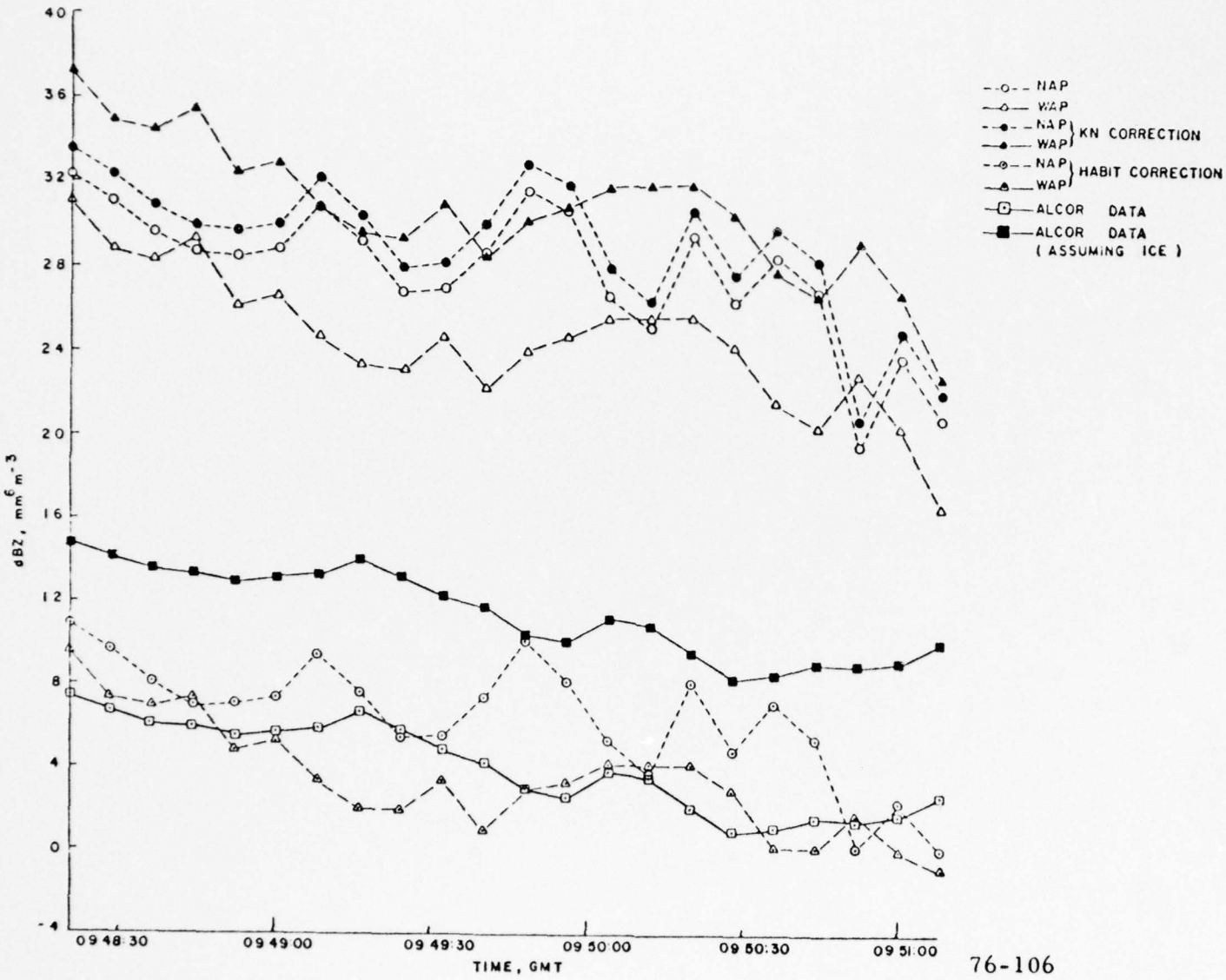

Figure 25. Time plots of dBZ in 8-second averages for radar and aircraft. Both original and corrected aircraft-calculated dBZ are shown. See legend for specifics.

It was shown that the DF problem does not alter the Z and WC results as severely as the UNSZ problem, the main reason being the difference in the affected size-classes. In the case of UNSZ the entire spectrum is affected, it is shifted; whereas, spectra having the DF problem lose particles from the small size end only. Except for very narrow spectra, the latter problem ranges from less significant to negligible in comparison with the former when Z and WC estimates are of principal concern.

It is felt that NAP is the appropriate probe to use for small particles. From this study, it can be concluded that WAP does a comparable job to NAP, once the corrections for undersizing and undercounting are applied. True number concentrations of the smallest particles are not recoverable with WAP without involving extrapolation techniques at the small-size end of the spectrum.

REFERENCES

Carbone, R. E., and R. C. Srivastava, 1975: Simultaneous aircraft and Doppler radar observations of a deep stratiform layer: Part II - Radar measurements and derived air motions. Proc. 16th Radar Meteor. Conf., 441-446.

Cunningham, R. M., 1975: Personal communication.

Davey, R. F., 1975: Comparison of cloud particle measuring techniques. Part I: Liquid water clouds. Part II: Ice crystal clouds. Report No. MRI 75 IR-1298 to DNA, Cont. DNA 001-74-C-0028.

Heymsfield, A. J., 1972: Ice crystal terminal velocities. J. Atmos. Sci., 29, 1348-1357.

Heymsfield, A. J., 1975: Simultaneous aircraft and Doppler radar measurements of a deep stratiform layer. Part I: Aircraft measurements and microphysical calculations. Proc. 16th Conf. Radar Mod., 433-440.

Heymsfield, A. J., 1975a: Precipitation development in stratiform ice clouds. Paper No. MRI 75 Pa-1376 to Air Force Geophysical Laboratories, 24 October 1975.

Knollenberg, R. G., 1975: The response of optical array spectrometer to ice and snow; A study of probe size to crystal mass relationships. Final Report AFCR-TR-75-0494 for Air Force Geophysical Labs by Particle Measuring Systems, 70 pp.

Locatelli, J. D., P. V. Hobbs, 1974: Fall speeds and masses of solid precipitation particles. J. Geophys. Res., 79, 2185-2197.

DISTRIBUTION LIST

DEPARTMENT OF DEFENSE

Defense Documentation Center
12 cy ATTN: TC

Director
Defense Intelligence Agency
ATTN: Tony Dorr, DIA-DT-2
ATTN: DI-7D
ATTN: DT-1C, Nuc. Eng. Br.
ATTN: DT-2, Wpns. & Sys. Div.

Director
Defense Nuclear Agency
ATTN: STVL
ATTN: STSI, Archives
ATTN: DDST
ATTN: RATN
ATTN: SPAS
3 cy ATTN: STTL, Tech. Lib.

Director of Defense Research & Engineering
ATTN: AD/S&SS
ATTN: DD/R&AT
ATTN: DD/S&SS
ATTN: AD/ET, J. Persh

Commander
Field Command
Defense Nuclear Agency
ATTN: FCPR, Colonel John P. Hill
ATTN: FCPR
ATTN: FCTMOF

Director
Joint Strategic Target Planning Staff, JCS
ATTN: JLTW-2
ATTN: JPTM
ATTN: JPTP
ATTN: JPST, G. D. Burton
ATTN: JPST

Chief
Livermore Division, Field Command, DNA
ATTN: FCPRL

OJCS/J-5
ATTN: J-5, Plans & Policy, R & D Div.

Studies Analysis & Gaming Agency
ATTN: SDEB

DEPARTMENT OF THE ARMY

Director
Ballistic Missile Defense Advanced Technical Center
ATTN: CRDABH-S

Program Manager
Ballistic Missile Defense Program Office
ATTN: John Shea
ATTN: DACS-BMT, Clifford E. McLain

Commander
Ballistic Missile Defense System Command
ATTN: BDMSC-TEN, Noah J. Hurst

DEPARTMENT OF THE ARMY (Continued)

Deputy Chief of Staff for Research, Development & Acq.
ATTN: NCB Division

Commander
Harry Diamond Laboratories
ATTN: DRXDO-NP, Francis N. Wimenitz
ATTN: DRXDO-NP

Commander
Picatinny Arsenal
ATTN: Al Loeb

Commander
TRASANA
ATTN: R. E. DeKinder, Jr.

Director
U.S. Army Ballistic Research Laboratories
ATTN: Richard Vitali
ATTN: Robert E. Eichelberger

Commander
U.S. Army Mat. & Mechanics Research Center
ATTN: DRXMR-HH, John F. Dignam

Commander
U.S. Army Materiel Dev. & Readiness Cmd.
ATTN: DRCDE-D, Lawrence Flynn

Commander
U.S. Army Missile Command
ATTN: DRSMI-RRR, Bud Gibson

Commander
U.S. Army Nuclear Agency
ATTN: ATCA-NAW

Chief
U.S. Army Research Office
ATTN: Consultant Peter P. Radowski

DEPARTMENT OF THE NAVY

Chief of Naval Operations
ATTN: Code 604C3, Robert Piacesi

Director
Naval Research Laboratory
ATTN: Code 5180, Mario A. Persechino

Commander
Naval Sea Systems Command
ATTN: ORD-0333A

Commander
Naval Surface Weapons Center
ATTN: Code WA-501, Navy Nuc. Prgms. Off.
ATTN: Code 323, W. Carson Lyons

Director
Strategic Systems Project Office
ATTN: NSP-27231, Marcus Meserole
ATTN: NSP-272, CDR Leslie Stoessl
ATTN: NSP-273
ATTN: NSP-27331, Phil Spector

DEPARTMENT OF THE AIR FORCE

Det. 30, 6 WWG
ATTN: Capt J. Thoma
ATTN: Capt F. Guiberson

AF Materials Laboratory, AFSC
ATTN: LPH, Gordon Griffith
ATTN: MBC, Donald L. Schmidt
ATTN: MBE, George F. Schmitt

AF Weapons Laboratory, AFSC
ATTN: DYT, Capt Daniel A. Matuska
ATTN: Maj Lawrence T. James
ATTN: SAB, Col George H. Dimon
ATTN: SUL

AFTAC
ATTN: Col Earnest F. Dukes, Jr.

Headquarters
Air Force Systems Command
ATTN: SOSS
ATTN: XRTO

Commander
Foreign Technology Division, AFSC
ATTN: TDFBD, J. D. Pumphrey

AF Geophysics Laboratory, AFSC
ATTN: LYC/LYW, C. Touart
ATTN: LYC/LYW, A. Barnes
ATTN: LY, Don McLeod
ATTN: LYC, Robert Cunningham
ATTN: Vernon G. Plank

HQ USAF/RD
ATTN: RDPM
ATTN: RDQPN
ATTN: David S. Hyman

HQ USAF/XO
ATTN: XOOSS, Capt George Nickols

SAMSO/MN
ATTN: MNN
ATTN: MNNA, Lt Col H. C. Lehman
2 cy ATTN: MNNR, Lt Col W. F. Villines
3 cy ATTN: MNNT, Lt Col D. Ricke

SAMSO/RS
ATTN: RSSE
ATTN: RSTP, Maj T. Speed, Capt F. Rapp
ATTN: RSSE, Lt A. T. Hopkins

Commander in Chief
Strategic Air Command
ATTN: XPQM, Maj Richard D. Ness
ATTN: XPFS, Lt Col Fleischmann
ATTN: DOXT

SAMSO/WE
ATTN: WE, Lt Col M. Keller

ENERGY RESEARCH & DEVELOPMENT ADMINISTRATION

Division of Military Application
U.S. Energy Research & Development Administration
ATTN: Doc. Con. for CDR Richard E. Peterson

ENERGY RESEARCH & DEVELOPMENT ADMINISTRATION (Continued)

University of California
Lawrence Livermore Laboratory
ATTN: R. Wagner, L-7
ATTN: Joseph B. Knox, L-216

Los Alamos Scientific Laboratory
ATTN: Doc. Con. for Donald Kerr
ATTN: Doc. Con. for Richard A. Gentry

Sandia Laboratories
Livermore Laboratory
ATTN: Doc. Con. for Thomas B. Cook, Org. 8000

Sandia Laboratories
ATTN: Doc. Con. for M. L. Merritt

DEPARTMENT OF DEFENSE CONTRACTORS

Acurex Corporation
ATTN: Robert M. Kendall

Aeronautical Rsch. Assoc. of Princeton, Inc.
ATTN: Coleman Donaldson

Aerospace Corporation
ATTN: J. McClelland
ATTN: R. Mortensen
ATTN: J. Niegen
ATTN: C. Glenn
ATTN: F. Barcatta

Applied Theory, Inc.
2 cy ATTN: John G. Trulio

Arcon Corporation
ATTN: H. G. Norment

Avco Research & Systems Group
ATTN: John Gilmore, E-502
ATTN: William G. Reinecke

Battelle Memorial Institute
ATTN: Richard Castle
ATTN: E. Unger

California Research & Technology, Inc.
ATTN: Ken Kreyenhagen

Calspan Corporation
ATTN: Romeo A. DeLiberis

University of Dayton
Industrial Security Super KL-505
ATTN: Hallock F. Swift

General Electric Company
Space Division
ATTN: Phillip Cline
ATTN: Don N. Vachon

General Electric Company
TEMPO-Center for Advanced Studies
ATTN: B. Gambill
ATTN: DASIAC

General Research Corporation
ATTN: John Ise, Jr.

DEPARTMENT OF DEFENSE CONTRACTORS (Continued)

Institute for Defense Analyses
ATTN: Joel Bengston

Kaman Sciences Corporation
ATTN: Jerry L. Harper

General Research Corporation
Washington Operations
ATTN: J. Belyea

LFE Corporation
Environmental Analysis Lab. Division
ATTN: Marcel Nathans

Lockheed Missiles & Space Co., Inc.
ATTN: Lawrence F. Hearne, Dept. 81-14

Martin Marietta Aerospace
Orlando Division
ATTN: James M. Potts, MP-121
ATTN: Joyce Hull
ATTN: William A. Gray

Meteorology Research, Inc.
ATTN: William D. Green
ATTN: E. Lobl
ATTN: A. J. Heymsfield
ATTN: R. E. Carbone
ATTN: L. J. Jahnsen

R & D Associates
ATTN: Cyrus P. Knowles
ATTN: F. A. Field
ATTN: Harold L. Brode

The Rand Corporation
ATTN: R. Robert Rapp

Raytheon Company
ATTN: Library

DEPARTMENT OF DEFENSE CONTRACTORS (Continued)

Science Applications, Inc.
ATTN: John Warner

Science Applications, Inc.
ATTN: J. Courtney

Stanford Research Institute
ATTN: Philip J. Dolan

TRW Systems Group
ATTN: Donald Jortner
ATTN: Peter Brandt

TRW Systems Group
San Bernardino Operations
ATTN: Earl W. Allen

TRW Systems Group
5 cy ATTN: R. A. Wilmot

TRW Systems Group
ATTN: R. Reeve, CADM